Dense Nonaqueous Phase Liquid (DNAPL) Source Zone Characterization in Highly Heterogeneous Permeability Fields

A Thesis

submitted by

Xinyu Wang

In partial fulfillment of the requirements

for the degree of

Master of Science

in

Civil and Environmental Engineering

TUFTS UNIVERSITY

February, 2013

Advisor: Dr. Linda M. Abriola, Dr. Itza Mendoza-Sanchez

Abstract

The characterization of DNAPL source zones provides important information for evaluating cost-effective remediation schemes at contaminated sites. In this work, numerical simulations were conducted to investigate the influence of: the capillary pressure-saturation parameters; residual organic saturation; spill rate; hypothetical field structure; and dimensionality on the DNAPL migration and entrapment simulation in a highly heterogeneous aquifer.

The results indicate that, in highly heterogeneous aquifers, the determination of capillary pressure-saturation parameters has a critical influence on the modeling of the DNAPL migration, while the residual organic saturation has almost no influence on DNAPL distributions. The spill rate strongly affects the DNAPL spread. The location of low permeability layers has critical consequences on the prediction of the vertical migration. The maximum organic saturation and pool fraction for highly heterogeneous aquifers are higher than those for mildly heterogeneous aquifers. The feasibility of using 2-D simulation results to predict 3-D simulation trends needs additional work.

Acknowledgements

I would first like to gratefully acknowledge my thesis committee members: Dr. Linda Abriola, Dr. Itza Mendoza-Sanchez, and Dr. Eric Miller. I would like to thank Dr. Linda Abriola for giving me the opportunity to conduct this research. This thesis was made possible due to her masterly guidance. I would like to deeply thank Dr. Itza Mendoza-Sanchez for her consistent diligence and patience to guide me through every detail during the process of my research and thesis writing. Without her help and encouragement, this thesis would never be possible. I am fortunate to have Linda and Itza as my advisors. I would like to thank Dr. Eric Miller for providing time and thoughtful comments which have helped me make progress on this thesis.

I would also like to acknowledge the faculty at the Department of Civil and Environmental Engineering and my classmates and friends at Tufts University. I would never forget the time we spent together doing our homework and preparing for the exams. I don't mention the names because there are so many of you. I would never forget the help I got from every one of you, and I wish to express my sincere thanks to all of you.

Lastly, I would like to thank my parents back home at China for their constant support and encouragement. They have always been the source of my inspiration throughout my life.

Table of Contents

List of Tables

List of Figures

Dense Nonaqueous Phase Liquid (DNAPL) Source Zone Characterization in Highly Heterogeneous Permeability Fields

Chapter 1: Introduction and Background

Dense non-aqueous phase liquids (DNAPLs) are fluids immiscible in water. As indicated by their name, they are chemicals or mixtures of chemicals that are denser than water. Commonly found DNAPLs include halogenated solvents, coal tar and creosote, and PCB oils (Cohen and Mercer, 1993). Among these chemicals, the most extensive subsurface contamination is associated with chlorinated solvents such as trichloroethylene (TCE), tetrachloroethylene (PCE), and trichloroethane (TCA).

In the past century, chlorinated solvents have been widely used as industrial solvents, degreasers, feedstocks, pesticides, and end products (NRC, 2004). After disposal, chlorinated solvents can be introduced into the subsurface through leaking tanks, leaking chemical distribution pipelines, and landfill disposal, among others (Pankow and Cherry, 1996). Due to the extensive production, transport, utilization, and disposal of large volumes of chlorinated solvents during the 20th Century, contamination of groundwater by these DNAPLs is substantial and widespread (US EPA, 1992).

Although the solubility of DNAPLs is very low (hundreds to thousands of ppm), these dissolved concentrations are considerably higher than the level that can cause negative impacts to the environment, ecology system, and human health (few to hundreds of ppb) (NRC, 2004). Negative impacts of DNAPLs on humans and animals include damage to the central nervous system, immune systems, liver, kidney, and mucous membranes, among others. For instance, studies on laboratory animals determined that PCE is

carcinogenic by inhalation and oral exposure; human health studies indicated that PCBs can increase cancer risk, disrupt reproductive functions, and cause neurobehavioral deficits in children (Irwin, 1997).

Once entrapped in the subsurface, DNAPLs are very difficult to completely remove from contaminated sites. The pure phase residual DNAPL in the aquifer matrix can act as a continuous source of dissolved contaminant, preventing the restoration of the affected aquifer zone to applicable water quality standards for tens or hundreds of years (US EPA, 1992). Therefore, the occurrence of trapped DNAPL in the subsurface has shown to be a significant limiting factor in groundwater remediation.

1.1 Infiltration and Entrapment

When released at the surface, DNAPL migrates under gravitational forces, moving into the open pores of the soil matrix. It tends to migrate vertically through the unsaturated zone and will encounter the saturated zone in which water completely fills the pore space. Upon reaching the saturated zone, if the hydraulic potential of the DNAPL exceeds the capillary force, it will continue its vertical migration, displacing the groundwater in the pores (Cohen and Mercer, 1993). The vertical migration ends when the DNAPL is unable to overcome the capillary entry pressure, often on the top of a low permeability layer, or when the volume of DNAPL is depleted (NRC, 2004; Pankow and Cherry, 1996).

During the migration and displacement process, a portion of the mobile DNAPL body will be entrapped due to the capillary trapping mechanism. In

the large pore openings, the entrapped DNAPL (non-wetting phase) will occur as disconnected blobs, while the wetting phase, water, fills the smaller pores and forms a film on the surface between the nonwetting DNAPL blobs and soil matrix (Newell et al., 1994). If enough DNAPL is present on the top of a low permeability layer, it will tend to spread horizontally and pool above the layer, until reaching the edge of the layer and finding new pathways to continue its vertical migration (Cohen and Mercer, 1993; Pankow and Cherry, 1996; Mayer and Hassanizadeh, 2005). After a significant portion of DNAPL is retained in porous media, the mobile DNAPL body will be depleted until it is finally exhausted. As a result of these processes, residual DNAPL will be retained in the saturated zone. The portion of a contaminated site affected by free-phase or residual DNAPL is often referred to as a source zone (US EPA, 1992). The source zone persists for a long period until it slowly dissolves into the groundwater passing through it, thus sustaining a contaminant plume down-gradient of the source zone within the subsurface regions.

1.2 Source Zone Architecture and Metrics

Generally, saturation (V_{DNAPL}/V_{Voids}) is used to define the characteristics and volumetric distribution of DNAPL, where V stands for the volume. Residual saturation, the saturation at which DNAPL is trapped by capillary force in the pores, is an important parameter in source zone characterization (Cohen and Mercer, 1993; Kueper and Frind, 1991a). The regions at which the saturation of DNAPL is greater than the maximum residual organic saturation are often referred to as pools, otherwise the regions are referred to as ganglia. The location of pools and ganglia, or the spatial distribution of DNAPL saturation,

is termed source zone architecture (Christ et al., 2006).

Previous investigations have found that the regions dominated by discrete ganglia generally produce higher but less sustained contaminant mass flux than those dominated by high-saturation pools (Parker and Park, 2004; Park and Parker, 2005; Christ et al., 2006, 2010). This is due to the fact that ganglia dominated regions have higher specific interfacial area and dissolve more rapidly than pools (Christ et al., 2010). Considering the different mass discharge behavior between the pools and ganglia, determination of the source zone architecture, as well as the fraction of pools and ganglia in the source zone, has important implications for site cleanup. For example, ganglia to pool ratio (GTP), and the pool fraction (PF) have been used as metrics to describe DNAPL dissolution duration and behavior (Christ et al., 2006, 2010; Difilippo and Brusseau, 2011). Other important metrics that have been used to describe the source zone architecture include: the location of the center of mass, the spread of mass, and the maximum organic saturation.

Numerous studies have reported the importance of the source zone characteristics on the prediction of down-gradient contaminant mass flux and persistence of the source, which have been used as measure for site remediation performance (Basu et al., 2006; Chris et al., 2006, 2010; Falta et al., 2005; Fure et al., 2006; Park and Parker, 2005; Wood et al., 2005). To date there is no single technology (e.g. pump-and-treat, in situ chemical oxidation/reduction, surfactant enhanced aquifer remediation) that removes all of the DNAPL from a contaminated site (Difilippo and Brusseau, 2011). To develop a technologically feasible and cost-effective remediation scheme that

combines several remediation technologies, it is necessary to estimate the initial mass and spatial extent of DNAPL at a contaminated site, or to quantify metrics that could be used to predict the duration and behavior of the DNAPL source zone dissolution.

1.3 Source Zone Characterization and Numerical Modeling

DNAPL source zone characterization provides the details of the spatial distribution of DNAPL saturation in the aquifer (Pantazidou and Liu, 2008). The determination of the DNAPL pathways in the subsurface is a complex task because they are highly dependent on the soil structure, while the field-scale heterogeneity is rarely recreated in the lab (Kueper et al., 1993; Kueper and Gerhard, 1995; Imhoff et al., 2003). In addition, accidental spills are difficult to characterize (Pouslen and Kueper, 1992; Kueper et al., 1993; Essaid et al., 1993), and systematic field experiments are generally prohibited (Kueper and Frind, 1991b; Christ et al., 2005). As a result, numerical simulations have become an important alternative for improving our understanding of DNAPL migration and entrapment in the subsurface (Abriola and Pinder, 1985, Kaluarachi and Parker, 1986; Kueper and Frind, 1991a; Essaid and Hess, 1993; Kueper and Gerhard, 1995).

A number of numerical models have been developed and demonstrated capable of simulating the migration and entrapment behavior of DNAPL through porous media (Abriola et al., 1992; Unger, 1995; UTCHEM, 2000; Park and Parker, 2005; Felta et al., 2005; Grant et al., 2007). Numerical studies have investigated the influence that model assumptions related to spatially variable physical properties (permeability, porosity, and capillary parameters)

have on the DNAPL infiltration process (Kueper and Frind, 1991b; Essaid and Hess, 1993; Kueper and Gerhard, 1995; Bradford et al., 1998; Dekker and Abriola, 2000; Lemke et al., 2004). Since the transport of DNAPL in the subsurface is known to be controlled by the heterogeneity of the soil structure, and because of the significant role that capillary pressure plays on the DNAPL migration process, model assumptions of soil properties and capillary parameters may strongly influence the simulation results (Dekker and Abriola, 2000; Kueper and Frind, 1991b; Rathfelder and Abriola, 1998; Essaid and Hess, 1993).

Kueper and Frind (1991b) examined the influence of soil heterogeneity on the lateral spreading of DNAPL by inserting a lower permeability lens into the spatially correlated heterogeneous permeability field. They performed two-dimensional (2-D) numerical simulations and demonstrated that DNAPL accumulates above the low-permeability layer and that the lateral spreading will be controlled by the horizontal correlation length of the low-permeability lens. They also found that migration of DNAPL is extremely sensitive to subtle changes in the capillary properties of the soil.

Lemke et al. (2004) investigated the influence of the determination of spatial correlation in porosity and permeability on predicted DNAPL distributions in a 2-D aquifer. They concluded that in spite of the significance of the soil heterogeneity, choices of geostatistical model (Sequential Gaussian Simulation (SGS), Sequential Indicator Simulation (SIS)) used to obtain the permeability and porosity field representation have minor influences on the organic distribution in the mildly heterogeneous aquifer. They also found that scaling

of capillary-pressure-saturation parameters to the permeability exerts a strong influence on predicted DNAPL spreading. This result is consistent with those presented by (Kueper and Frind, 1991b; Essaid and Hess, 1993, Decker and Abriola, 2000; Christ et al., 2005), all of which are conducted in mildly heterogeneous permeability fields (σ^2_{lnk}ranges from 0.14-1.0).

A number of three dimensional (3-D) numerical simulations of DNAPL infiltration and entrapment in relatively homogeneous glacial outwash sands have been conducted, but few of them resulted in the presence of a large number of high saturation pools (Lemke and Abriola, 2006; Park and Parker, 2005; Parker and Park, 2004; Christ et al., 2010). Christ et al (2010) suggested that one possible reason for the lack of pooling is that the geostatistical simulation approaches (e.g., SGS, SIS) used to generate the non-uniform hydraulic conductivity field do not preserve sufficient textural contrast and laterally continuous stratigraphy (Christ et al., 2010; Lee et al., 2007). To study the dissolving behavior in a high-pooling source zone, they used two approaches: (1) created hypothetical lateral continuous low permeability layers by inserting extensive, thin low permeability lenses (K=min(K) in the domain) in a mildly heterogeneous permeability field; and (2) emplaced DNAPL high-pool source zones along the bottom layer of their numerical domain. These approaches eventually produced relatively high PF (0.30 to 0.56) in their aquifer domains.

Apart from the soil properties, Essaid and Hess (1993) suggested that the migration behavior also depends on the fluid saturations ($k_{ro} = f(S_w, S_t)$, where k_{ro} is the relative permeability), if the hysteresis due to organic

entrapment is incorporated. Dekker and Abriola (2000) studied the effects of the correlation of residual organic/water saturations with permeability on DNAPL entrapment behavior in a heterogeneous 2-D aquifer ($\sigma^2_{lnk} = 0.24$). Their results demonstrated that predictions of DNAPL infiltration are insensitive to the correlation of residual water and organic saturations with soil permeability. They explained this result by analyzing the hysteretic residual organic expression given by Land (1968) ($\bar{S}_{or} = \frac{1-\bar{S}_w^{min}}{1+R(1-\bar{S}_w^{min})}$ and $R = \frac{1-S_{wr}}{S_{or}^{max}} - 1$). They observed that at low values of the maximum organic residual saturation, the sensitivity of the organic residual to its maximum value decreases, and concluded that at the low simulated values of maximum DNAPL saturation in the Borden sand formation (below 0.3), no significant effect of correlation between the permeability field and the residual organic saturation is expected. In highly-heterogeneous fields, since a much higher maximum historical organic saturation is expected, the influence of the correlation of residual organic saturation with permeability is anticipated to play a more important role. In addition, they reported a strong effect of spill rate on organic distribution in this aquifer and observed a decrease in lateral spreading and vertical penetration, as well as an increase in maximum organic saturation at higher DNAPL release rates. They also suggested that the influence of the spill rate may not be as critical in a more heterogeneous formation for predictions of the DNAPL distribution.

Previous studies on source zone characterization and hydraulic property influence on DNAPL distribution were primarily based upon the mildly heterogeneous aquifers, such as the Bachman road site studied by Lemke et al.

(2004) and the Borden aquifer studied by Dekker and Abriola (2000). In these studies, SGS was generally used to obtain the permeability field, and high textual contrast and laterally continuous stratigraphy were not present. In the present study, a highly heterogeneous glaciofluvial deposit aquifer is studied, of which the major differences with the former studied aquifer are (1) greater lateral extent of the low permeability layers across the domain; (2) larger range of permeability values (four orders of magnitude comparing with one order of magnitude); (3) higher contrast between contiguous layers. From the conclusions of Kueper and Frind (1991b) and Christ et al. (2010), it is reasonable to infer that extensive pooling can occur in this highly heterogeneous aquifer.

Maji (2005) employed a transition-probability-based Markov Chain (TP/MC) model to reconstruct this 3-D highly heterogeneous glaciofluvial deposit aquifer. He showed that the TP/MC method successfully preserved the lateral continuity of the permeability field and achieved higher mean DNAPL saturations in this realistic highly-heterogeneous natural formation, comparing with those work performed in the relatively homogeneous aquifer (Christ et al., 2006, 2010; Lemke et al., 2004, 2006; Kueper and Frind, 1991b).

Maji et al. (2006) employed both TP/MC and the traditional variogram analysis to reconstruct the DNAPL source zone architecture and the aqueous-phase plume configuration by sampling the saturation and TCE mole fraction data from the forward simulation results in one permeability field. For different conditioning cases, they produced 20 saturation and aqueous-phase mole fraction realizations with the TP/MC approach and calculated their

ensemble mean. Then they compared the TP/MC mean to the results from only one single realization obtained with ordinary kriging that used a fitted exponential variogram model. They proved the accuracy and flexibility of the TP/MC approach for aquifer and contaminant plume reconstruction and concluded that the TP/MC is preferable compared to ordinary kriging for the DNAPL source zone and dissolved contaminant plumes reconstruction.

Maji and Sudicky (2008) studied the effects of various mass transfer correlation models for DNAPL dissolution in a highly heterogeneous aquifer and explored the benefits of partial mass removal in this aquifer. They generated 20 (3-D) realizations of the aquifer analog for each dissolution model using the TP/MC method that was conditioned using all the available hydraulic data. They found that the dissolution models developed based on relatively homogeneous aquifer materials in the laboratory experiments yielded vastly different time frames for complete DNAPL source zone removal in the highly heterogeneous aquifer, and the benefits of partial source-zone remediation were highly dependent on the local-scale dissolution processes. In spite of these studies in a highly heterogeneous aquifer, the influences of the soil characteristics (capillary pressure parameters, residual saturation) on the migration and entrapment of DNAPL in the subsurface were not systematically investigated.

Previous studies have found that it is possible to approximate the 3-D source zone architecture with 2-D simulation results (Liu, 2001; Christ et al., 2005). Liu (2001) reported good agreement between 2-D radial symmetric and 3-D simulation results of DNAPL flow in a relatively homogeneous permeability

field. Christ et al. (2005) found that in statistically homogeneous non-uniform field, the DNAPL distribution metrics obtained by 2-D and 3-D field-scale simulations are correlated. In order to study the influence of soil characteristics on the DNAPL infiltration and entrapment process in the highly heterogeneous aquifer, the present study focuses on 2-D simulations due to considerable savings in computational time. The simulated results will be compared with previous studies reported for 2-D mildly heterogeneous permeability fields. Recognizing that for more heterogeneous formations, 2-D simulations may not result in good representation of more realistic 3-D metrics (Christ et al., 2005), selected 2-D simulations will be compared to their 3-D analogs.

Chapter 2: Objectives, Goals and Hypotheses

2.1 Objectives

The overall objective for this study is to systematically investigate the influence of input parameters, permeability field distribution and dimensionality on simulated DNAPL entrapment and infiltration behavior in the subsurface of a highly heterogeneous aquifer. The specific goals are: (1) to explore the influence of capillary pressure-saturation parameters and the effects of the determination of residual organic saturation on the simulation of DNAPL entrapment in the highly heterogeneous aquifer; (2) to investigate the influence of different hypothetical spill rate scenarios on DNAPL migration in the highly heterogeneous aquifer; (3) to study the influence of hypothetical permeability field structures on the DNAPL entrapment behavior; (4) to investigate the ability to extend the conclusion based on 2-D simulations to 3-D simulations by comparing selected 2-D and 3-D simulations; (5) to compare the DNAPL entrapment and infiltration behavior with that for mildly heterogeneous aquifers, the simulated results for each task here will be compared to former studies as discussed in Chapter 1 (Dekker and Abriola, 2000; Lemke et al., 2004; Christ et al., 2005).

2.2 Goals and Hypotheses

Goal 1: To investigate the influence of capillary pressure-saturation parameters and residual organic saturations

To attain goal 1, two alternative approaches were used to determine the capillary pressure-saturation parameters—Leverett scaling and Haverkamp and Parlange Method (HPM)—as will be explained in Chapter 3. Similarly, two alternatives for residual organic saturations were employed to explore the influence of residual organic saturation on DNAPL infiltration in the highly heterogeneous aquifer. One alternative assumes that residual organic saturation is independent of permeability, while the other one assumes a correlation between residual organic saturation and permeability. Then simulations were conducted with different sets of combinations of capillary pressure-saturation parameters and residual organic saturations. Finally, simulated results were compared to investigate the influence of capillary pressure parameters and residual organic saturations on DNAPL distribution in a highly heterogeneous aquifer.

Hypothesis 1: The capillary pressure-saturation parameters have strong influence on the simulation of DNAPL infiltration and entrapment within the highly heterogeneous aquifer. The correlation of residual saturation parameters to the permeability also strongly influences DNAPL migration in the subsurface of this highly heterogeneous aquifer.

Goal 2: To investigate the influence of spill rates

The spill rate was demonstrated to strongly influence the DNAPL migration in

mildly heterogeneous aquifers. To attain goal 2, three spill rates were adopted to explore the effects of spill rate on the DNAPL migration in the highly heterogeneous aquifer. Namely slow release (0.5 L/day), medium release (2 L/day), and fast release (5 L/day).

Hypothesis 2: The spill rate has strong influence on DNAPL entrapment behavior in highly heterogeneous permeability fields. The same trend with the results for mildly heterogeneous aquifers is expected, i.e., with increasing spill rate, more mass would tend to be concentrated in the center areas thus less spreading would occur.

Goal 3: To investigate the effects of hypothetical field structures

To attain goal 3, two different hypothetical field structures were studied. In the first permeability field (hypothetical field 1), low permeability capillary barriers are present on the top of the domain around the release area of DNAPL. In the other permeability field (hypothetical field 2), low permeability layers are present at deeper regions without surrounding the release points. In this way, the influence of the field structures on the prediction of each metric was explored.

Hypothesis 3: The permeability field structure will influence the predictions for several metrics for the DNAPL distribution in the highly heterogeneous permeability field. The TP/MC method that is employed to reconstruct the highly heterogeneous permeability field should be used with caution.

Goal 4: To compare 2-D and 3-D simulation results

To attain goal 4, predictions of DNAPL infiltration and entrapment in 3-D

versus 2-D aquifers were conducted. Comparison between 2-D and 3-D simulation results were used to explore the feasibility to extend conclusions based on 2-D simulations to 3-D simulations.

Hypothesis 4: The dimensionality will highly affect the DNAPL entrapment and infiltration behavior, due to the highly connected layers in the *x* and *y* direction. The metrics predicted by 2-D and 3-D simulations will be different.

Goal 5: To compare simulated results for highly heterogeneous aquifer with that for mildly heterogeneous aquifer

Heterogeneity has been demonstrated to significantly influence DNAPL pathways and entrapment behavior in the subsurface in numerical studies that have been performed based upon relatively homogeneous or mildly heterogeneous aquifers. However, few studies have investigated the factors that have strong effects on the entrapment and infiltration behavior of organic liquids in highly heterogeneous aquifers. To attained goal 5, the simulation results from goal 1 to goal 4 will be compared with results for previous studies for mildly heterogeneous aquifers (Dekker and Abriola, 2000; Lemke et al., 2004; Christ et al., 2005).

Hypothesis 5: In highly heterogeneous aquifers where continuous stratigraphy and sufficient textural contrast are present, larger extent of pooling will occur than that within mildly heterogeneous aquifers. Meanwhile, much higher values for maximum organic saturation than those for mildly heterogeneous aquifers will be achieved. Other metrics, like horizontal spread and vertical penetration, predicted in highly heterogeneous aquifer will also be different with those in mildly heterogeneous aquifers.

Chapter 3: Methodology

To accomplish the main objective, simulations of DNAPL migration and entrapment will be conducted in multiple realizations. For this, 3-D realizations of a highly heterogeneous permeability field will be reconstructed. Then 2-D permeability fields will be obtained by extracting the *x*-*z* center cross section from the 3-D domain. Multiple 2-D permeability realizations will be employed to obtain an ensemble of simulations and to compute the ensemble's DNAPL distribution statistics. Different cases of DNAPL infiltration simulations that incorporate different aquifer property characteristics and spill conditions will be defined. To evaluate the influence of capillary pressure-saturation (Pc-sat) parameters, the ensemble will incorporate Pc-sat parameters independent of and dependent on permeability of the soils. To investigate the influence of organic residual saturation, the ensemble will include organic residual saturations uncorrelated and correlated to permeability values. Three different hypothetical spill scenarios will be simulated for the ensembles, namely fast, medium, and slow release rate of the DNAPL. The influence of capillary pressure parameters and organic saturation in different spill scenarios will be quantified by obtaining DNAPL distribution statistics of selected metrics (center of mass and spread along vertical and lateral directions, GTP and PF, maximum organic saturation) for each simulation case and obtaining the differences among these statistics.

3.1 Site of investigation and reconstruction

The studied aquifer is located at Southwest Germany, 500 meters west of the town of Herten. Researchers at the University of T$\ddot{u}$bingen, Germany (Heinz et al., 2002; Kostic et al., 2005; Bayer et al., 2011) obtained a high-resolution aquifer analog dataset through intensive data collection. Following Heinz et al. (2003) and the aquifer analog, Maji (2005) defined four dominant lithofacies types and categorized them based on genetic description and hydraulic parameters (Table 3.1).

Table 3.1 Soil Properties at Herten Site

Lithofacies	Description	Volumetric Proportion	Permeability (m2)	Porosity
Gs-x	Well-sorted gravel	29%	5.14×10^{-12}	0.2
Gcm	Poorly-sorted gravel	57%	2.63×10^{-11}	0.23
S-x	Pure,well-sorted sand	6%	1.14×10^{-10}	0.24
bGcm,i	Cobble-and boulder-rich gravel	6%	1.49×10^{-8}	0.26

Geostatistical reconstruction of the T$\ddot{u}$bingen aquifer at Herten site was conducted by Maji (2005) and is used in the present work. The reconstruction employs a transition-probability-based Markov Chain (TP/MC) approach that was demonstrated robust and accurate for mapping aquifer facies patterns within the aquifer analog (Maji, 2005). The transition probability $t_{jk}(\mathrm{h})$ is defined as the probability that a quantity of category *j* occurs at location *x*, given that the same (or another) quantity of category *k* occurs at location *x*+*h*:

$$t_{jk}(\mathrm{h}) = \Pr\{k\ occurs\ at\ x + h |\ j\ occurs\ at\ x\} \quad (1)$$

where *h* is the lag, and *j* and *k* are two different categories of geologic facies.

Markov chains analysis gives a transition probability matrix T(Δh) that can be used as a geostatistical model of spatial variability (Carle, 1999).

The transition probability matrices (Table 3.2) for this study were reported by Maji (2005) and were based on the conditioning points collected by University of T*ü*bingen. The off-diagonal entries of the matrices are the transition probabilities from one category to another, while the diagonal entries represent the mean thickness of each facies body in meters. Further details on the generation of the transition probability matrix can be found in Maji (2005).

Table 3.2 Transition Probability Matrices in the Respective Direction

	x-direction				y-direction				z-direction			
	Gs-x	Gcm	S-x	bGcm,i	Gs-x	Gcm	S-x	bGcm,i	Gs-x	Gcm	S-x	bGcm,i
Gs-x	3.6	0.17	0.53	0.31	7.1	0.002	0.51	0.48	0.3	0.37	0.43	0.2
Gcm	0.15	14.6	0.51	0.33	0.34	9.8	0.51	0.15	0.53	0.9	0.3	0.17
S-x	0.41	0.3	0.78	0.29	0.48	0.33	1.5	0.19	0.71	0.29	0.1	0.001
bGcm,i	0.65	0.04	0.31	1.12	0.31	0.39	0.3	2.2	0.66	0.33	0.01	0.2

In this study the Transition Probability Geostatistical Software (T-PROGS 2.1) (Carle, 1999) was used to obtain geostatistical simulations of the Herten site. The transition probability matrix for the four dominant lithofacies reported in Maji (2005) was used as an input in T-PROGS to generate a series of 3-D realizations of spatial variability of the 4 lithofacies. A Markov Chain model for the 4 lithofacies was developed by means of interpretation of transition rates relative to the embedded transition probability matrix obtained from Maji (2005). A first unconditional categorical simulation was generated based on the Markov Chain model obtained. The categorical field simulation was generated for a 16×10×7 m aquifer region discretized into 179200 cells that have grid dimensions of 0.25×0.5×0.05 m in the *x*, *y* and *z* directions respectively. This resolution is similar to that used in Maji et al. (2006) and small relative to the mean thickness of the facies bodies in all directions

(smallest thickness of 0.1 m for S-x in *z* direction) to permit adequate resolution of the permeability distribution in all directions.

Following the first categorical realization a set of 18 randomly located hypothetical boreholes with 0.25 m spacing in the z-direction were chosen to sample categorical data. The number of conditioning points was demonstrated by Maji (2005) to be enough to preserve the aquifer properties during reconstructions. The final set of 3-D categorical realizations (20 realizations) were conditionally generated using the Markov Chain model and the boreholes data obtained. Thus, the first categorical realization was used as a hypothetical categorical field, where borehole samples defined as "observed" values were obtained and the subsequent categorical realizations are equally probable spatial distributions that honor the "observed" data at the sampling locations. In this study 2 different hypothetical categorical fields or hypothetical field sites were generated in order to study the influence of the aquifer formation on DNAPL source architecture simulated. Therefore in order to obtain DNAPL distribution statistics of ensembles of 20 realizations, a total of 40 conditional categorical realizations were generated and used in DNAPL simulations; 20 realizations conditioned based on hypothetical field 1 (HF1) and 20 more conditioned based on hypothetical field 2 (HF2).

Rathfelder and Abriola (1998) stated that the accurate simulation of long-term DNAPL redistribution requires a fine vertical grid structure that is one-fifth to one-tenth of the entry pressure height, thus reasonable convergence in the simulations can be obtained. To achieve this, the vertical grid size in this study should be 5 to 10 times smaller than the smallest entry pressure Pb, which is

0.7 cm as indicated by Table 3.5. However, with a grid of the size of 0.7 cm, 1000 nodes are required in the vertical direction (the vertical scale is 7 m for the studied domain), which will make the computation almost impossible in terms of CPU demand. As a result, a coarser resolution was necessary for computational efficiency with the large number of simulations required in this study.

The grid resolution that uses a reasonable amount of CPU time was determined by analyzing simulations with different vertical refinement. Figure 3.1 (a) depicts a simulation based on a resolution of 0.25×0.05 m and Figure 3.1 (b) illustrates the resulting simulation with a coarser vertical resolution of 0.25×0.1 m. Both simulations were conducted with the same volume of DNAPL (80 L) released into the ground at the same spill rate (2 L/day). Observable differences in the simulated metrics for different resolutions exist as listed in Table 3.3, especially for GTP and PF. However, both simulations exhibit a similar trend of the DNAPL pathway and location of pools in the domain. In addition, the coarser vertical grid resolution (10 cm) requires only 70 nodes in the vertical direction, which saves a large amount of CPU effort. Thus the coarser grid size will be used in this work for the reason of large amount of computer efforts required in this study.

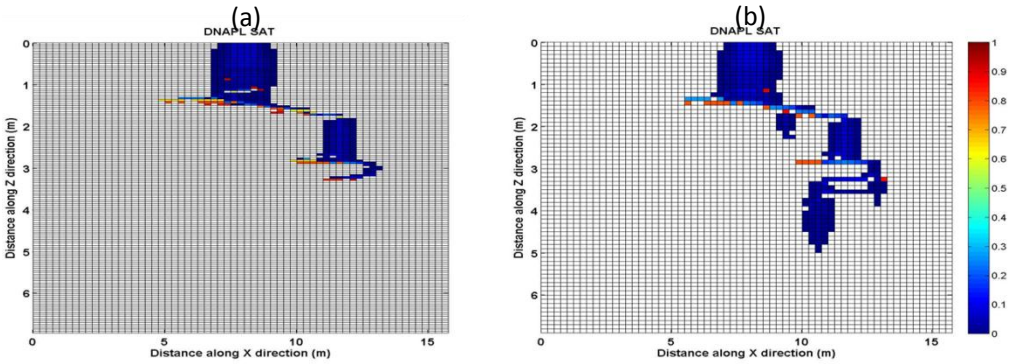

Figure 3.1 DNAPL source zone architecture with a) original resolution and b) coarser resolution

Table 3.3 Estimation for metrics with original resolution and coarser resolution

Vertical Grid Spacing (m)	Max saturation	x center of mass	z center of mass	x spread	z spread	GTP	PF
0.05	0.92	8.828	1.715	4.079	0.689	0.327	0.754
0.1	0.904	9.124	1.823	3.774	0.815	0.804	0.554

In this work, the two lithofacies (S-x and bGcm,i) that account for the high permeability and low entry pressure values take only 12% of the total volume for the studied aquifer, thus it is reasonable to ignore the extremely fine resolution required by these two lithofacies.

After the 3-D realization with coarser resolution in the vertical direction (0.25x0.5x0.1m) was obtained, 2-D categorical realizations were obtained by extracting the *x*-*z* center cross section of the 3-D domain as shown in Figure 3.2.

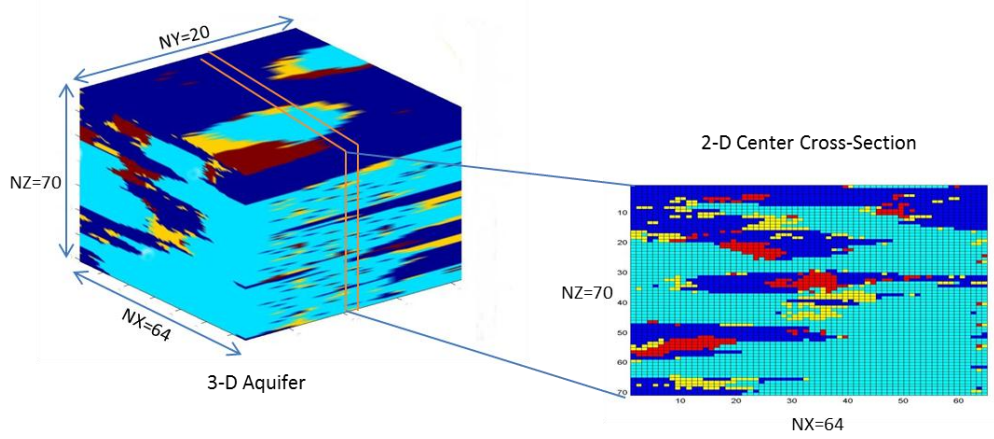

Figure 3.2 Field Reconstruction—Conceptualization for Obtaining the 2-D Permeability Field

Figure 3.3 (a) to (d) and 3.3 (e) to (h) depict 4 examples of aquifer realizations by soil category (1 to 4) for field 1 and field 2 respectively, which demonstrates the performance of TP/MC method to reconstruct the highly heterogeneous Herten aquifer with sufficient lateral continuous stratigraphy. Stratification is evidenced by a higher degree of continuity in the horizontal versus the vertical direction.

As mentioned previously, conditioning points were taken from 18 hypothetical boreholes randomly located in 3-D hypothetical field 1 (HF1). The locations of the hypothetical boreholes, which served as the "observed" data for each set of 3-D realizations, are shown in Figure 3.3. Figure 3.4 contains 2-D profiles extracted from the 3-D permeability fields, (Figure 3.4 (a) for HF1 and 3.4 (e) for HF2) and subsequent realizations (Figure 3.4 (b) to (d) for HF1 and 3.4 (f) to (h) for HF2) are positioned in similar locations in the domain.

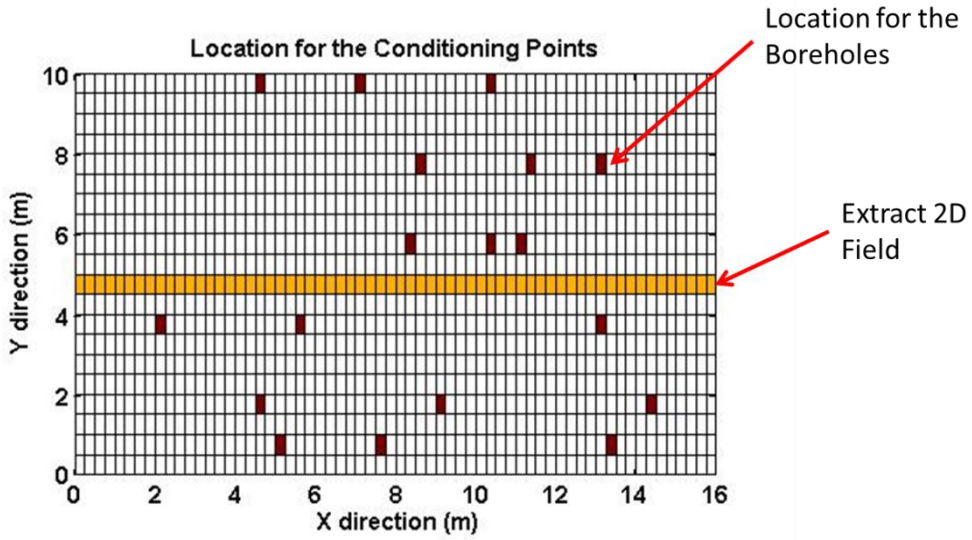

Figure 3.3 Locations of the Hypothetical Boreholes

Figure 3.3 is a top view for the 3-D domain, which shows the locations for the randomly located hypothetical boreholes. Within each borehole, a 0.25 m spacing in the z-direction were chosen to sample the categorical data. Therefore, there are a total of 504 conditioning points within the entire 3-D domain.

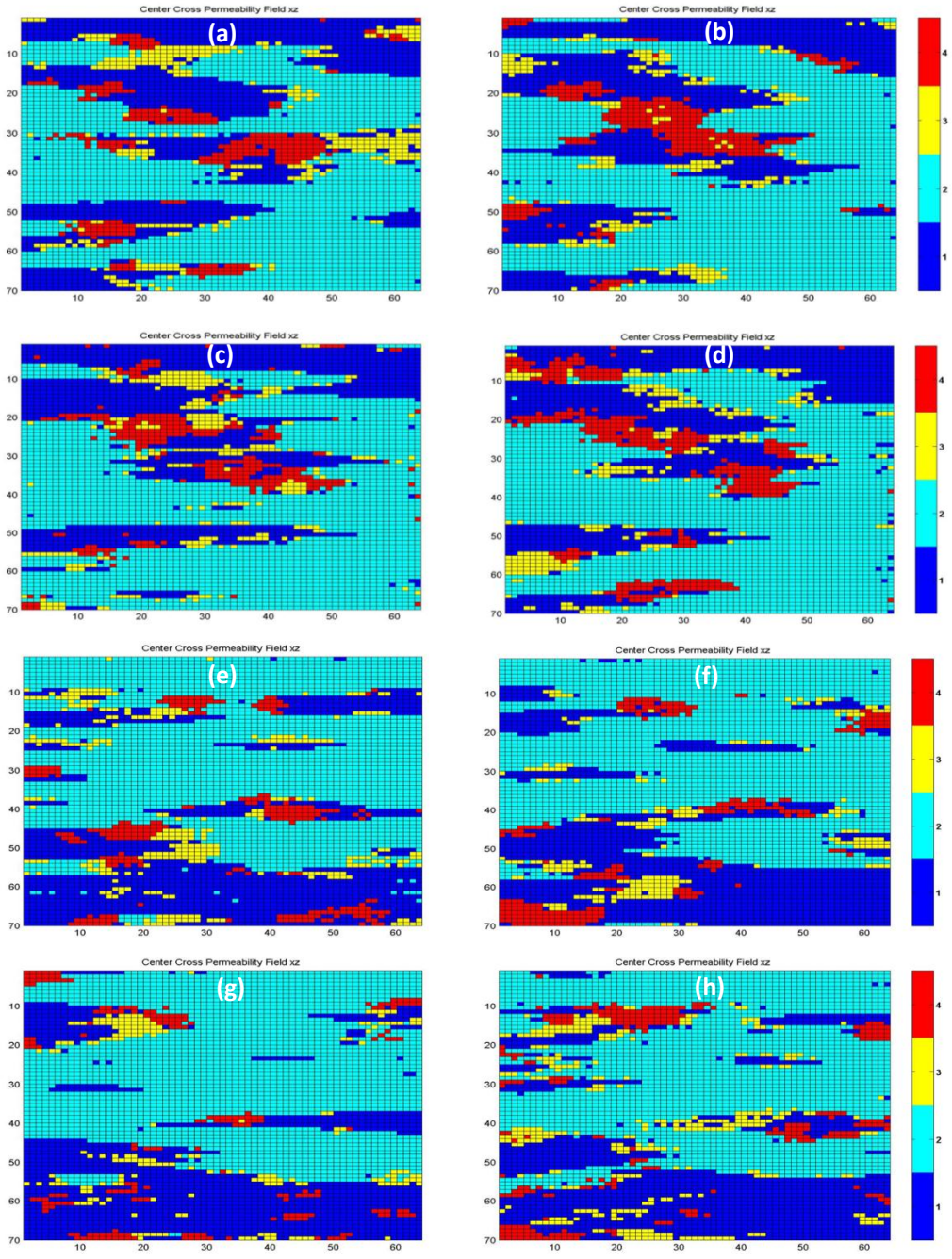

Figure 3.4 Examples of 2-D Permeability (a) Hypothetical field 1, (b to d) subsequent HF1 realizations; (e) Hypothetical Field 2, and (f to h) subsequent HF2 realizations. The formations are similar due to conditioning data. Lateral continuous stratigraphies are observed

3.2 Numerical simulations

To investigate the influence of capillary pressure parameters, the correlation of organic residual saturation with the permeability field, the spill rate, and the hypothetical field structure on the DNAPL infiltration and entrapment behavior in the highly heterogeneous aquifer, two-dimensional numerical simulations were performed using an existing multiphase flow simulator, Michigan Vertical and Lateral Organic Redistribution (M-VALOR) (Abriola et al., 1992; Rathfelder and Abriola, 1998).

M-VALOR solves governing equation combining two phase mass balance equations with Darcy's equation and incorporates constitutive equations describing capillary pressure-saturation relationships and hysteresis (Abriola et al., 1992). The governing equation for DNAPL infiltration obtained by combining the mass balance equation with Darcy's equation for multiphase flow is:

$$\frac{\partial}{\partial \mathrm{t}}(\Phi S_\alpha \rho_\alpha) = \nabla \cdot \left(\frac{k k_{r\alpha}}{\mu_\alpha} \nabla (P_\alpha - \rho_\alpha \mathrm{gz}) \right) + q_\alpha \qquad (2)$$

where Φ stands for the porosity, S_α is the saturation of α-phase, ρ_α is the density of α-phase, q_α represents external sources/sinks, κ is the soil intrinsic permeability tensor, $k_{r\alpha}$ is the relative permeability of α-phase fluid, μ_α is the dynamic viscosity, and P_α is the α-phase fluid pressure.

In this study, only two fluid phases are taken into consideration (water and DNAPL). Therefore, the constraint that

$$S_w + S_o = 1.0 \qquad (3)$$

has to be met (Abriola et al., 1992; Lemke et al., 2004).

This study employs the Brooks-Corey Model to determine the Pc-Sat relationship for primary drainage (Brooks and Corey, 1964).

$$\bar{S}_w = \left(\frac{P_b}{P_c}\right)^{\lambda} \qquad \text{if} \quad P_c \geq P_b \tag{4}$$

$$\bar{S}_w = 1.0 \qquad \text{if} \quad P_c \leq P_b$$

where $\bar{S}_w$ is the effective water saturation, P_c is the capillary pressure, P_b is the entry or bubbling pressure, and λ is the pore size distribution index. Following Kaluarachchi and Parker (1992) hysteresis and entrapment are incorporated by substituting the effective water saturation in (4) with the apparent effective water saturation $\bar{\bar{S}}_w$ when saturation is along any imbibition scanning curve. $\bar{\bar{S}}_w$ is assumed to be a simple function of capillary pressure which incorporates hysteresis and entrapment. It is defined by the sum of effective water saturation $\bar{S}_w$ and the normalized trapped or immobile organic phase saturation $\bar{S}_{ot}$:

$$\bar{\bar{S}}_w = \bar{S}_w + \bar{S}_{ot} \tag{5}$$

The normalized trapped or immobile organic phase saturation follows Lenhard et al. (1989) and is given by:

$$\bar{S}_{ot} = \bar{S}_{or}\left(\frac{\bar{S}_w - \bar{S}_w^{min}}{(1-\bar{S}_{or}) - \bar{S}_w^{min}}\right) \tag{6}$$

where $\bar{S}_{or}$ is the effective residual DNAPL along the scanning imbibition curve originating at the minimum effective water saturation prior imbibition ($\bar{S}_w^{min}$) on the primary drainage curve and is calculated with the Land (1968)

equation:

$$\bar{S}_{or} = \frac{1-\bar{S}_w^{min}}{1+R(1-\bar{S}_w^{min})} \quad \text{and} \quad R = \frac{1-S_{wr}}{S_{or}^{max}} - 1 \tag{7}$$

Finally, the Brooks-Corey (1964) relative permeability functions are used (Lemke et al., 2004):

$$k_{rw} = \bar{S}_w^{\frac{2+3\lambda}{\lambda}} \tag{8}$$

$$k_{ro} = \left(1 - \bar{\bar{S}}_w\right)^2 \left(1 - \bar{\bar{S}}_w^{\frac{2+\lambda}{\lambda}}\right) \tag{9}$$

Equation (2) for each phase with the constitutive relations (Eqn. (3) to (9)) and the initial and boundary conditions constitute a well-posed problem which can be solved numerically. The finite difference code M-VALOR solves the system of equations through an iterative implicit pressure-explicit saturation scheme. This scheme first solves a single pressure equation implicitly (with P_w=P_o), and afterwards applies the updated pressures through an explicitly time stepping methods to solve the mass balance equations for fluid saturations (Rathfelder and Abriola, 1998; Demond et al., 1996).

In this study, a DNAPL (PCE) will be released from 4 nodes at the top of the permeability field located at the center along x direction. Impermeable boundaries are defined at the top and bottom of the studied domain. Summaries of the input parameters of the simulations are given in the following section.

3.3 Input Parameters

Table 3.4 summarizes the base scenario input parameters (case 1) for the simulations. In the case 1 simulation, residual organic saturation is set to be

uniform in the domain. Reference air entry pressure P_b^{ref} and pore size index λ are estimated from background category's (Gcm) grain size distribution curves (obtained from Heinz et al., 2003) with known porosity (0.23) and assumed dry bulk density for sands. The background category Gcm is the poorly-sorted gravel and contains the largest volumetric portion in the studied aquifer (57%). The method employed to calculate the P_b^{ref} and the λ for Gcm is given by Haverkamp and Parlange (1986) (HPM).

Table 3.4 Numerical Simulation Input Parameters (Base Scenario)

Parameter		
Fluid Properties	**Water**	**PCE**
Density (Kg/m^3)	999.0032^a	1625^a
Dynamic viscosity (Pa·s)	0.1121×10^{-2a}	0.89×10^{-3a}
Compressibility (1/Pa)	4.4×10^{-10a}	0.0^a
Initial saturation	1	0
Residual saturation	0.08^a	0.235^b (uniform)
Capillary pressure-saturation Parameters		
Reference entry pressure Pb (Pa)	1667.73^c(for Gcm)	
Pore size index λ	2.33^c (uniform)	
Interfacial tension		
Air/water (dyne/cm)	72.75^a	
Air/PCE (dyne/cm)	34.5^a	
PCE/water (dyne/cm)	47.8^a	

[a]Christ et al., 2005
[b]Fit to match data of Hoag and Marley (1986)
[c]Fit to match method of Haverkamp and Parlange (1986)

Table 3.5 gives the spatially variable capillary pressure-saturation parameters for the four lithofacies obtained by two alternative approaches. The first alternative is the commonly used Leverett scaling (Leverett, 1941) that scales the entry pressure by intrinsic permeability and porosity values:

$$P_b = P_b^{ref} \sqrt{\frac{k^{ref} \emptyset}{k \emptyset^{ref}}} \quad (10)$$

Previous studies have demonstrated minor influence of the variation in porosity on the DNAPL infiltration behavior (Lemke et al., 2004). Since the porosity values for different lithofacies are close in the studied aquifer (0.20 to 0.26), a uniform porosity (0.23) is assumed in this study. The pore size index λ is assumed uniform in the base case simulation to keep the shape of capillary pressure-saturation curve. In this case, a complete correlation between the entry pressure and the permeability will be achieved.

Another approach to derive the capillary pressure-saturation parameters is to use the HPM separately for each soil category estimated from their grain size distribution curves with known porosity and dry bulk density obtained from Heinz et al. (2003). This approach results in a decrease in the dependence of capillary pressure-saturation parameters on the permeability.

Table 3.5 Pc-Sat Parameters Obtained through Leverett Scaling and HPM

Lithofacies	Pore Size Index λ		Air Entry Pressure Pb (Pa)	
	Leverett Scaling	HPM	Leverett Scaling	HPM
Gs-x	2.33	1.86	3770.37	2261.25
Gcm	2.33	2.33	1667.73	1667.73
S-x	2.33	3.26	799.82	1125.48
bGcm,i	2.33	3.26	70.15	98.45

A negative log-linear correlation of S_{or} and permeability has been reported by Hoag and Marley (1986) and Powers et al. (1992), respectively. Dekker and Abriola (2000) presented regression models based on their data and used these models to predict S_{or} on the study of Borden aquifer. Since the majority of

the range of permeability for the Herten aquifer overlaps with that given by Hoag and Marley (1986), this study employs the regression model developed from their data by Dekker and Abriola (2000) to predict organic residual saturation. This regression model is given in Figure 3.5.

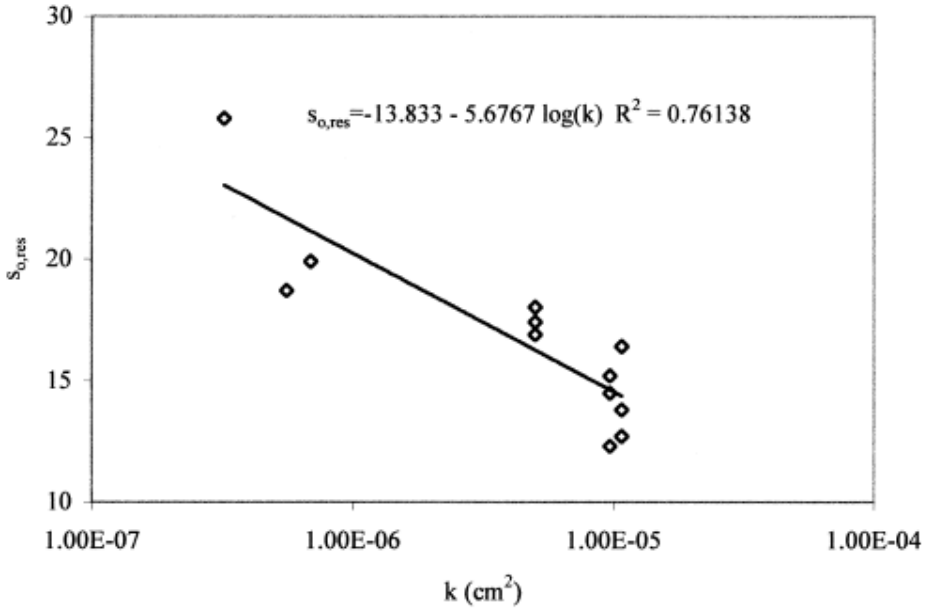

Figure 3.5 Correlation of Residual Organic Saturation with Aquifer Permeability -- based on data from Hoag and Marley (1986). Figure taken from Dekker and Abriola (2000)

Based on the capillary pressure-saturation parameters, the residual organic saturations, the spill rates, and the field structures, ten ensemble cases were generated to achieve the objective of this study. Each ensemble set contained the same number of the realizations of permeability field to perform simulations and obtain values of the source zone configuration metrics. Table 3.6 lists the simulation conditions for each case, with the same DNAPL released volume into the domain.

Table 3.6 Ten Alternative Simulation Cases

	Pb	Lambda	Residual Organic Saturation	Spill Rate	Hypothetical Field	Abbreviation
Case 1 (Base Scenario)	Leverett Scaling	uniform	uniform	Medium （2L/day）	1	LS-1Sor-M-1
Case 2	HPM	HPM	uniform	Medium （2L/day）	1	HPM-1Sor-M-1
Case 3	Leverett Scaling	Uniform	correlated with permeability	Medium （2L/day）	1	LS-4Sor-M-1
Case 4	HPM	HPM	correlated with permeability	Medium （2L/day）	1	HPM-4Sor-M-1
Case 5	Leverett Scaling	Uniform	uniform	Slow (0.5L/day)	1	LS-1Sor-S-1
Case 6	HPM	HPM	uniform	Slow (0.5L/day)	1	HPM-1Sor-S-1
Case 7	Leverett Scaling	Uniform	uniform	Medium （2L/day）	2	LS-1Sor-M-2
Case 8	HPM	HPM	uniform	Medium （2L/day）	2	HPM-1Sor-M-2
Case 9	Leverett Scaling	uniform	uniform	Fast （20L/day）	1	LS-1Sor-F-1
Case 10	HPM	HPM	uniform	Fast （20L/day）	1	HPM-1Sor-F-1

Preliminary screening simulations with the base case conditions were conducted. Figure 3.6 (b) and 3.5 (c) depict examples for the organic distributions under the release volume of 25 L and 80 L, respectively. Here, both simulations of PCE infiltration were conducted in the same permeability realization (Figure 3.6 (a)) under the same spill rates of 2 L/day (0.5 L/day per node). Sufficient redistribution time (40 days in general) was allowed for the organic to reach a stable distribution state.

Clearly, at a low spill volume (25 L), DNAPL penetration depth is shallow and cannot provide sufficient insight to study the influence of different Pc-sat and residual organic saturation in the aquifer of interest. When a larger spill volume of 80 L is used in the simulation, DNAPL successfully penetrates to the bottom part of the domain and a complex DNAPL source architecture can

be observed. The large DNAPL volume inside the simulation domain allows for a better understanding of the influence of different parameters in this heterogeneous permeability structure. Following the screening simulations, all the simulations were conducted at a spill volume of 80 L, with three spill rates.

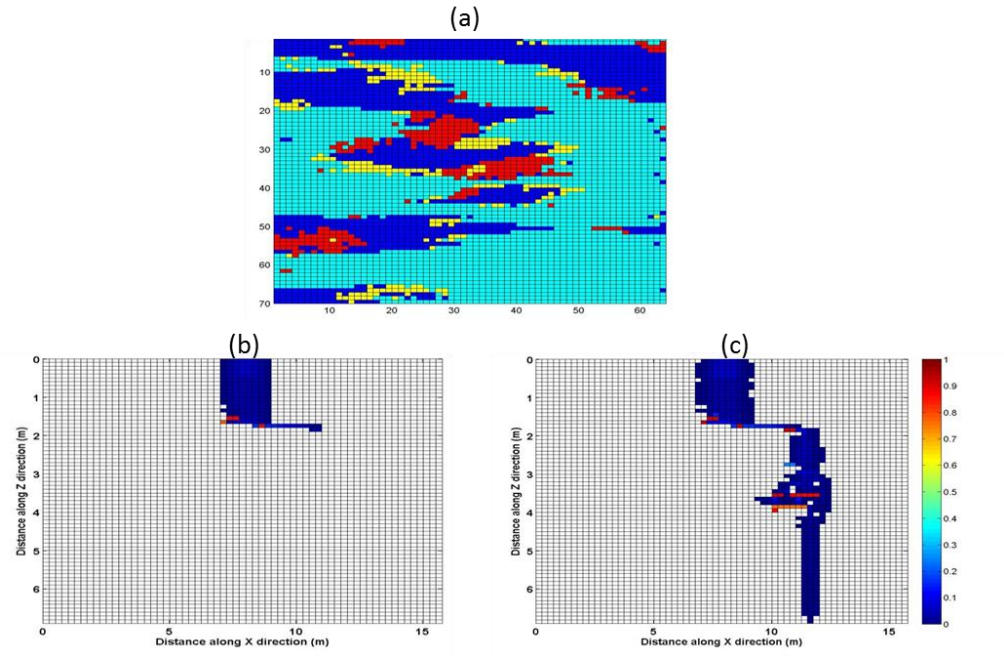

Figure 3.6 Simulated DNAPL Saturation Distribution (a) 2-D Permeability field realization; (b) Source zone architecture for a 25 L release at 2L/day; (c) Source zone architecture for a 80 L release at 2L/day

3.4 DNAPL distribution statistics

Since the differences between individual realizations will lead to a range of variability for the simulated results, multiple realizations are required to cover the range of variability. For each case in Table 3.6, an ensemble of simulations of DNAPL entrapment will be conducted in a specific number of realizations of the permeability field. The number of realizations is defined based on

examining the number of realizations needed to obtain stable estimations for the mean and variance of DNAPL source zone metrics in this highly heterogeneous system.

Studies on the relatively homogeneous Borden aquifer found that when the number of realizations exceeds 15, a stable estimate of variance for the simulated results can be observed (Dekker and Abriola, 2000; Lemke et al., 2004). Figure 3.7 illustrates an example of the mean and variance of the vertical spreading (σ_{zz}^2) estimated for increasing number of realizations in the highly heterogeneous Herten aquifer. It can be seen that the mean and variance for the vertical spread converge to a single value at sets of 15 or more realizations. For each individual simulation, about 2-15 hours of CPU time was required. This computational demand provides a limitation to the number of realizations, thus this study generated 20 realizations for each case of simulation to investigate the DNAPL infiltration and entrapment behavior in the subsurface.

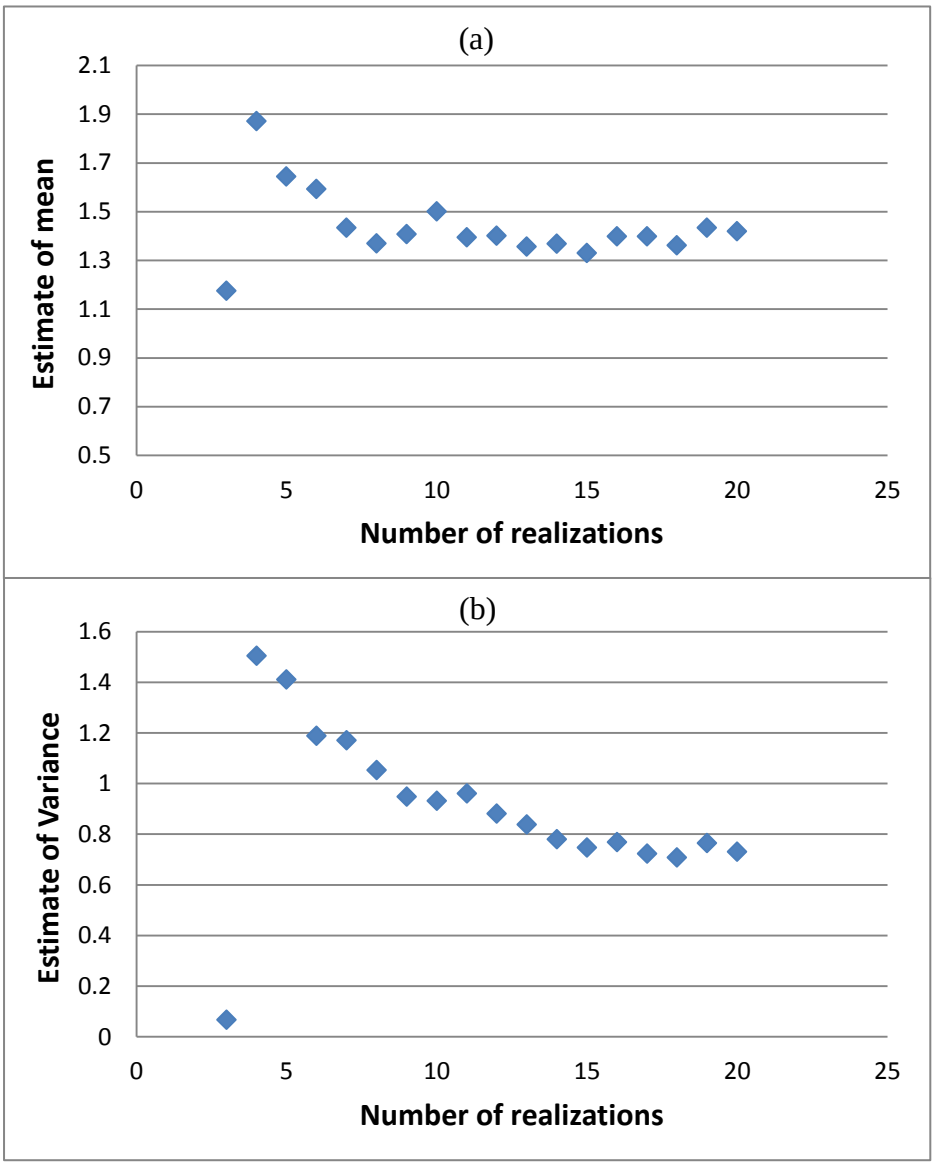

Figure 3.7 Estimate of the (a) Mean (b) Variance of σ_{zz}^2 for the Herten Aquifer

Each simulation gives detailed information of saturation distribution in the 2-D permeability field realization. Based on the saturation distribution, the source zone configuration metrics can be calculated with equation (11) through equation (15).

The GTP and the PF can be calculated as (Christ et al., 2006):

$$\text{GTP} = \frac{\sum \rho_o s_o \Phi \Delta x \Delta y \Delta z \forall s_o < s_{or}^{max}}{\sum \rho_o s_o \Phi \Delta x \Delta y \Delta z \forall s_o \geq s_{or}^{max}} = \frac{\sum s_o \forall s_o < s_{or}^{max}}{\sum s_o \forall s_o \geq s_{or}^{max}} \qquad (11)$$

and

$$\text{PF} = \frac{\sum \rho_o s_o \Phi \Delta x \Delta y \Delta z \forall s_o \geq s_{or}^{max}}{\sum \rho_o s_o \Phi \Delta x \Delta y \Delta z} = \frac{\sum s_o \forall s_o \geq s_{or}^{max}}{\sum s_o} \quad (12)$$

where ρ_o is the DNAPL density, Φ is the porosity, and s_{or}^{max} is the maximum residual organic saturation, the threshold used to distinguish between ganglia- and pool-dominated regions. For the simulation cases where s_{or}^{max} is correlated to permeability, GTP and PF were calculated taking into account the value of s_{or}^{max} used for each soil type. The GTP is unbounded, which means that if all mass is presented in ganglia, the GTP will be infinity, while the PF is bounded between 0 and 1.

Given the saturation distribution, spatial moments can be calculated following Kueper and Frind (1991b) and Essaid and Hess (1993):

$$M_{ij} = \int_{-\infty}^{\infty} \int_{-\infty}^{\infty} \Phi \rho_o S_o(x,z) x^i z^j \, dxdz \quad (13)$$

The zeroth moment M_{00} represents total mass of DNAPL in the domain. A measure of horizontal and vertical location for the center of DNAPL mass can be presented as:

$$x_{cm} = \frac{M_{10}}{M_{00}} \text{ and } z_{cm} = \frac{M_{01}}{M_{00}} \quad (14)$$

Similarly, the horizontal and vertical spreading of mass are given by:

$$\sigma_{xx}^2 = \frac{M_{20}}{M_{00}} - x_{cm}^2 \text{ and } \sigma_{zz}^2 = \frac{M_{02}}{M_{00}} - z_{cm}^2 \quad (15)$$

After multiple simulations are conducted for each simulation case in Table 3.6, the mean and variance of the metrics will be calculated. Finally, the differences among the resulting mean and variance of the metrics can be

quantified for the ten cases, and the influence of capillary pressure parameters, residual organic saturations, spill rates, and hypothetical field structures will be assessed.

Apart from studying the influence of capillary pressure parameters, residual organic saturations, spill rates, and hypothetical field structures on the DNAPL distribution in the heterogeneous aquifer, additional work was conducted to explore the DNAPL infiltration behavior in the subsurface with increasing heterogeneity by comparing the simulated results in this work with that reported by studies on mildly heterogeneous aquifers (Lemke et al., 2004; Dekker and Abriola, 2000). Lemke et al (2004) studied a 30×10 m source zone at the Bachman Road site. Dekker and Abriola (2000) studied the aquifer at Borden site comprised by a 5×10 m vertical cross-section, and the 2-D aquifer at Herten site studied here is a 16×7 m domain. Accordingly, in order to make the metrics comparable, namely the center of mass and DNAPL spread, it is necessary to convert them into dimensionless quantities. For this, the center of mass is divided by the corresponding scale for the respective domain, and the DNAPL spread is divided by the square length of related scale. With the similar grid refinement comparing to former studies, as discussed above, other metrics, like the maximum organic saturation, the GTP, and the PF are dimensionless, and thus, need not be transformed.

Chapter 4: Results and Discussion

4.1 General trend of DNAPL pathways and summary for source zone metrics

Figure 4.1 shows a profile with simulated PCE saturation distribution that is most representative of the mean ensemble value for the suite of realizations for the base scenario. Consistent with previous studies (Dekker and Abriola, 2000; Lemke et al., 2004; Christ et al., 2005), this profile shows the influence of aquifer hydraulic properties on the DNAPL migration pathways. The extensive low permeability layers occurring laterally across the domain form capillary barriers for DNAPL to continue its vertical movement. As a consequence, DNAPL tends to migrate horizontally and accumulate above low permeability layers, until a new pathway appears to allow for the vertical movement.

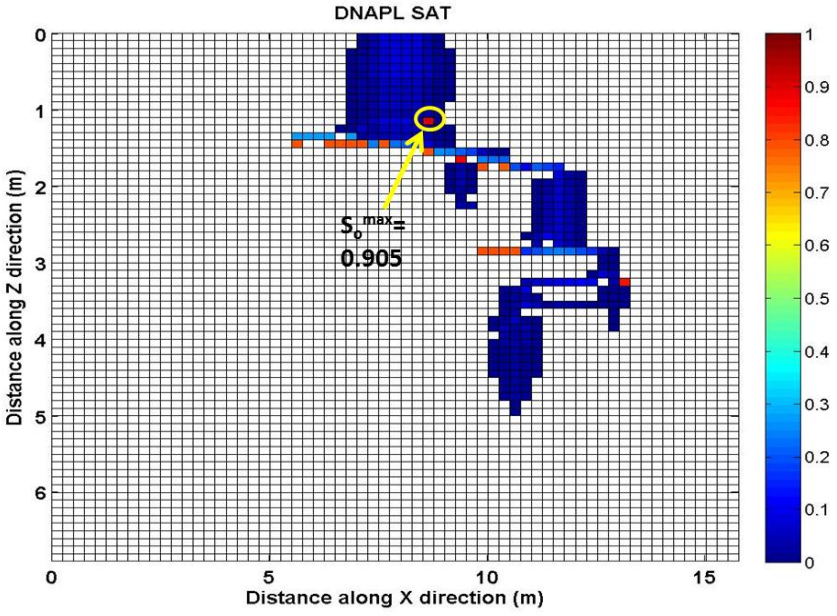

Figure 4.1 DNAPL Saturation Distributions in Representative 2-D Profiles

Figure 4.1 also shows the location at which the highest DNAPL saturation

occurs. DNAPL forms higher saturation pools here because at this location a high permeability soil is surrounded by a low permeability soil, thus when DNAPL enters this area, extensive lateral movement cannot occur.

Table 4.1 Summary of ensemble statistics for PCE distribution metrics

		s_o^{max}	x_{cm}	z_{cm}	σ_{xx}^2	σ_{zz}^2	GTP	PF
case 1	min	0.781	6.430	1.080	1.190	0.248	0.314	0.278
	max	0.917	10.400	3.820	6.160	6.580	2.590	0.761
LS-1Sor-M-1	mean	0.898	8.924	2.126	3.841	1.623	0.992	0.531
	stdev	0.041	0.964	0.652	1.358	1.488	0.554	0.117
case 2	min	0.911	6.310	1.470	0.264	0.664	0.433	0.149
	max	0.919	8.530	3.650	3.460	4.520	5.720	0.698
HPM-1Sor-M-1	mean	0.918	7.522	2.629	1.213	2.148	1.646	0.451
	stdev	0.002	0.630	0.535	0.737	1.184	1.396	0.160
case 3	min	0.780	6.390	1.080	1.190	0.248	0.318	0.279
	max	0.917	10.400	3.830	6.190	6.640	2.590	0.759
LS-4Sor-M-1	mean	0.897	8.924	2.139	3.876	1.685	1.005	0.530
	stdev	0.041	0.967	0.652	1.356	1.485	0.587	0.119
case 4	min	0.911	6.440	1.470	0.262	0.691	0.439	0.148
	max	0.919	8.530	3.630	3.480	4.560	5.760	0.695
HPM-4Sor-M-1	mean	0.918	7.556	2.590	1.212	2.118	1.608	0.458
	stdev	0.002	0.575	0.517	0.756	1.185	1.409	0.158
case 5	min	0.776	5.790	1.200	1.550	0.344	0.271	0.365
	max	0.918	10.700	4.420	8.650	6.850	1.740	0.787
LS-1Sor-S-1	mean	0.902	8.994	2.590	4.867	2.415	0.872	0.557
	stdev	0.042	1.319	0.755	1.908	1.796	0.395	0.117
case 6	min	0.913	6.210	1.760	0.559	0.787	0.248	0.343
	max	0.919	8.580	4.600	3.430	6.010	1.920	0.802
HPM-1Sor-S-1	mean	0.918	7.428	3.173	1.638	2.947	1.005	0.532
	stdev	0.001	0.708	0.728	0.804	1.605	0.525	0.137
case 7	min	0.787	6.730	1.600	0.633	0.607	0.403	0.150
	max	0.917	9.800	3.890	9.500	3.600	5.670	0.713
LS-1Sor-M-2	mean	0.896	8.205	2.926	2.968	2.056	1.563	0.437
	stdev	0.040	0.940	0.618	2.261	0.775	1.129	0.130
case 8	min	0.825	6.230	1.760	0.230	1.220	0.325	0.092
	max	0.919	8.840	4.250	4.820	4.480	9.880	0.755
HPM-1Sor-M-2	mean	0.912	7.707	3.398	0.980	3.105	2.268	0.365
	stdev	0.021	0.625	0.700	1.077	0.937	1.967	0.135
case 9	min	0.676	6.620	0.793	0.976	0.209	0.636	0.232
	max	0.916	9.250	2.110	3.350	2.980	3.310	0.611
LS-1Sor-F-1	mean	0.889	8.297	1.498	2.100	0.792	1.364	0.444
	stdev	0.056	0.707	0.356	0.749	0.599	0.617	0.091
case 10	min	0.506	6.630	1.070	0.245	0.381	0.920	0.147
	max	0.918	8.140	2.090	3.460	1.650	5.800	0.521
HPM-1Sor-F-1	mean	0.893	7.676	1.769	0.866	1.058	2.532	0.313
	stdev	0.092	0.428	0.252	0.710	0.350	1.192	0.100

Table 4.1 summarizes the ensemble maximum, minimum, mean and standard deviation values for the source zone configuration metrics, including

maximum PCE saturation (s_o^{max}), horizontal and vertical center of mass (x_{cm} and z_{cm}), horizontal and vertical spread (σ_{xx}^2 and σ_{zz}^2), GTP, and PF, for all simulation cases.

Case 1 to case 4 have cross combinations for two sets of capillary pressure-saturation parameters (obtained either by Leverett scaling or by Haverkamp and Parlange Method) and two sets of residual organic saturations (either uniform or correlated with permeability). The rest of the input parameters for case 1 to case 4 are identical. Inspecting the results for the first four cases, notable distinctions for the minimum, maximum, and mean value can be found for each metric with different sets of capillary pressure-saturation parameters, which demonstrates the influence of capillary pressure-saturation parameters on the simulation of DNAPL migration. However, the predictions of each metric with different sets of residual organic saturation are so similar that the influence of residual organic saturation can almost be neglected.

Comparing the results for case 1, case 5, and case 9 (or case 2, case 6, and case 10), where the only difference of the input parameters is the spill rate, a decreasing trend with increasing spill rate can be observed for s_o^{max}, σ_{xx}^2, z_{cm}, σ_{zz}^2. Clearly, the spill rate does influence the penetration and spread of DNAPL.

Comparing the results of each metric for case 1 and case 7 (or case 2 and case 8), it can be seen that the most pronounced influence of hypothetical field structure is on z_{cm} and σ_{zz}^2. The predictions of GTP and PF are also strongly affected by hypothetical field structure.

In general, the simulation results for PCE distribution reveal that residual organic saturations have minor influence on PCE infiltration and entrapment behavior compared to the capillary pressure-saturation parameters, release rate, and the permeability field structure. A strong influence of capillary pressure-saturation parameters, spill rates, and hypothetical field structure can be observed on σ_{xx}^2, σ_{zz}^2, GTP, and PF. x_{cm} is strongly influenced by capillary pressure-saturation parameters; z_{cm} is affected mainly by spill rates and hypothetical field structures; and s_o^{max} is sensitive mostly to capillary pressure-saturation parameters and spill rates. Notice that there are interplays between the capillary pressure parameters, spill rates, and hypothetical field structure. Therefore more detailed analysis will be performed and explained by individual goals in the following part.

4.2 Goal 1: Influence of capillary pressure-saturation parameters and residual organic saturations

In order to explore the effects of capillary pressure-saturation parameter selection in the Brooks-Corey model and the correlation of residual organic saturation with the permeability field on the simulation of PCE migration, task 1 uses the first four ensembles of simulation cases. As explained in chapter 3, case 1 and case 3 employ Leverett scaling, while case 2 and case 4 employ HPM. In case 1 and case 3, the residual organic saturation is uniform all over the permeability field. In case 2 and case 4, maximum residual organic saturation is correlated with the permeability, thus there are four different values for maximum residual organic saturation corresponding to the four different lithofacies.

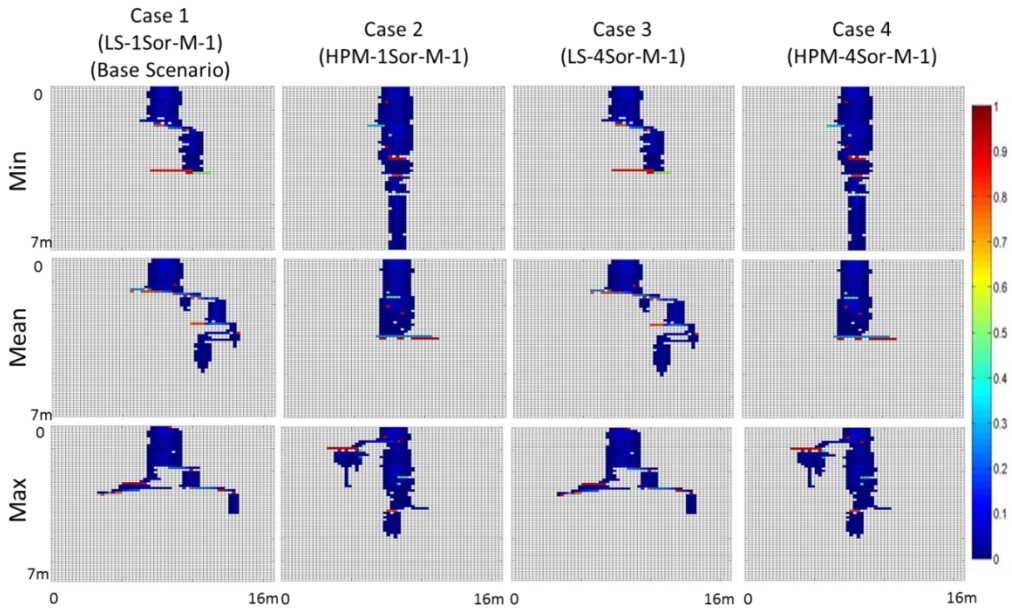

Figure 4.2 Representative PCE saturation distributions for simulation case 1 to case 4

Figure 4.2 depicts three representative PCE saturation distributions for cases 1 to 4. From top to bottom, the representative simulation results from the 20

simulations for the minimum, the value closest to the mean, and the maximum horizontal spread were chosen and present in each row for cases 1 to 4, respectively. This way to present these PCE pathways in this study is same with that used in Lemke et al. (2004). In this way, the similarity and differences for PCE pathways between each case can be easily observed. the Inspecting the different PCE migration pathways for case 1 and case 2, or case 3 and case 4, where the only difference is the determination of capillary pressure-saturation parameters, it can be seen that the assignment of capillary pressure-saturation parameters (either Leverett scaling or HPM) strongly affects the PCE entrapment and infiltration behavior. With Leverett scaling, there is a higher contrast of entry pressure between the extensive layers of lithofacies than that of HPM, which makes it more difficult for the PCE to penetrate through the low permeability layer. As a result, with Leverett scaling, the PCE has a higher tendency to move horizontally. With HPM, the contrast of entry pressure between layers is lower, thus it is easier for the PCE to pass through these capillary barriers and a marked decrease in horizontal movement can be observed.

Conversely, although the residual organic saturation is uncorrelated with permeability in case 1 and correlated with permeability in case 3, these two cases exhibit remarkably similar results (case 2 and case 4 which used HPM revealed the same trend). This indicates that the residual organic saturation has a very small influence on the DNAPL infiltration and entrapment behavior simulation.

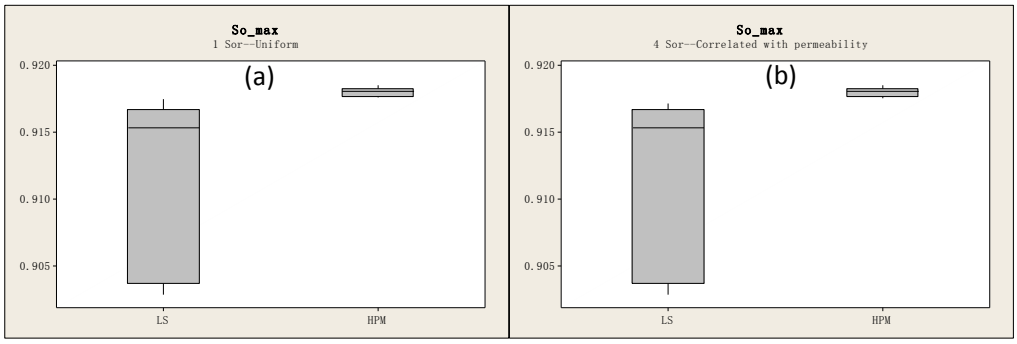

Figure 4.3 Sensitivity of s_o^{max} to capillary pressure-saturation parameters with a) uniform maximum residual organic saturation, and b) maximum residual saturation correlated to permeability

Figure 4.3 to Figure 4.6 are boxplots for the simulated metrics in case 1 to case 4, which describe the distribution of the metrics for multiple realizations in each simulated case. These boxplots can offer a more detailed explanation for cases 1 to 4. The line within the box locates the median value, and the upper and lower boundary of the box represents the 25% and 75% quartile, respectively. The ends of the whiskers are the maximum and minimum values.

Figure 4.3 illustrates the range of maximum PCE saturation (s_o^{max}) for cases 1 to 4, which share the same release rate but differ in the assignment of the capillary pressure-saturation and the residual organic saturation parameters. It can be seen that the range of simulated s_o^{max} value is quite small, most particularly for HPM. Statistical analysis suggests that with Leverett scaling the mean value for s_o^{max} is only about 2% smaller than that with HPM, but the range for s_o^{max} with Leverett scaling is approximately 95% higher than that with HPM. When using HPM, the ranges for s_o^{max} are extremely small, no matter how the residual organic saturation values are defined. No obvious differences are present for cases employing uniform residual organic saturations and varying residual organic saturations correlated with

permeability.

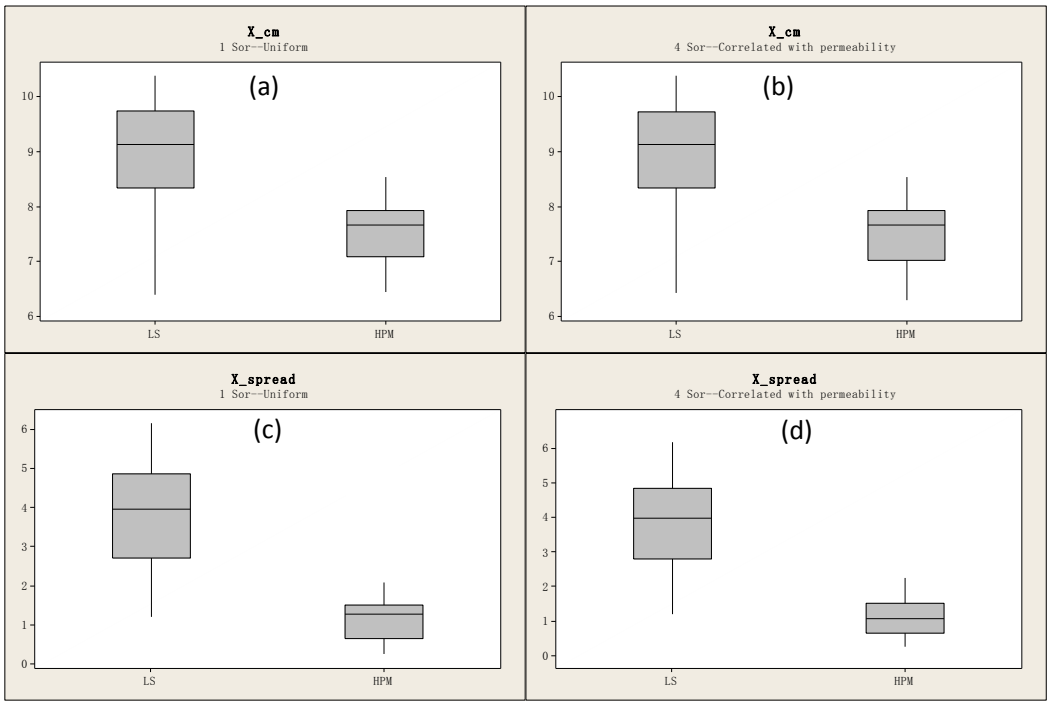

Figure 4.4 Sensitivity of x_{cm} and σ_{xx}^2 to capillary pressure-saturation parameters with a,c) uniform residual organic saturation and b,d) residual organic saturation with permeability

Figure 4.4 presents the influence of capillary pressure-saturation parameters and residual organic saturations on PCE distribution along the horizontal direction. The horizontal scale of the simulation domain is 16 m, thus the horizontal center of the domain is 8 m. It can be seen that with Leverett scaling and HPM, the center of PCE mass (x_{cm}) tends to be locatesd at different sides of the center of horizontal domain, which reflects different PCE migration pathways with Leverett scaling and HPM. Thus the prediction of x_{cm} is influenced by the determination of capillary pressure-saturation parameters.

Similarly, the prediction of horizontal spread σ_{xx}^2 with Leverett scaling is approximately 40% to 70% larger than that with HPM. In addition, with Leverett scaling, the range of σ_{xx}^2 tends to be about 50% larger than that with HPM. Therefore, the influence of capillary pressure-saturation parameters on

the prediction of σ_{xx}^2 is also strong.

However, comparing Figure 4.4 (a) to (b) (or Figure 4.4 c to d), the predictions for x_{cm} (or σ_{xx}^2) are so close that there is a negligible difference between them, indicating that the degree of maximum residual organic saturation correlation has no discernible influence on these parameters.

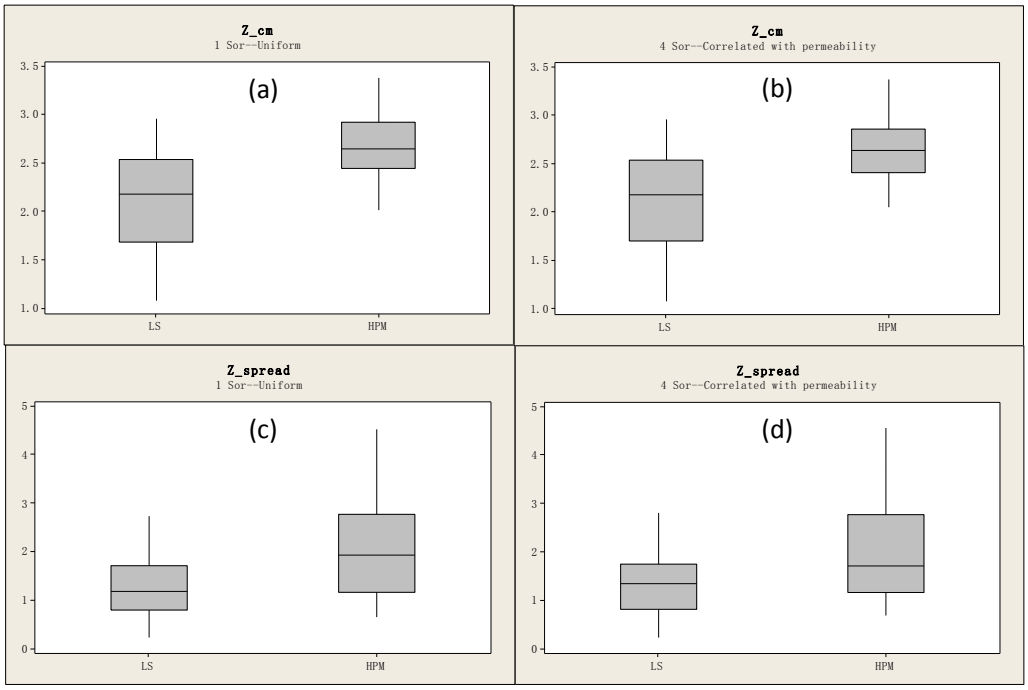

Figure 4.5 Sensitivity of z_{cm} and σ_{zz}^2 to capillary pressure-saturation parameters with a,c) uniform residual organic saturation and b,d) residual saturation correlated to permeability

Figure 4.5 illustrates the metrics that describe the vertical movement of PCE for case 1 to case 4, namely vertical center of mass (z_{cm}) and vertical spread σ_{zz}^2. Compared to Leverett scaling, an approximately 10% to 30% increase in z_{cm} and a 20% to 40% increase in σ_{zz}^2 can be observed with HPM, which means that with HPM the PCE tends to penetrate deeper into the subsurface and have a greater extent of vertical spread.

On the other hand, whether the residual organic saturation is uniform or correlated with permeability, the resulting z_{cm} and σ_{zz}^2 do not reveal obvious

differences. This result was observed with both sets of capillary pressure-saturation parameters. Thus, the selected maximum residual organic saturation does not have strong influence on the PCE vertical movement.

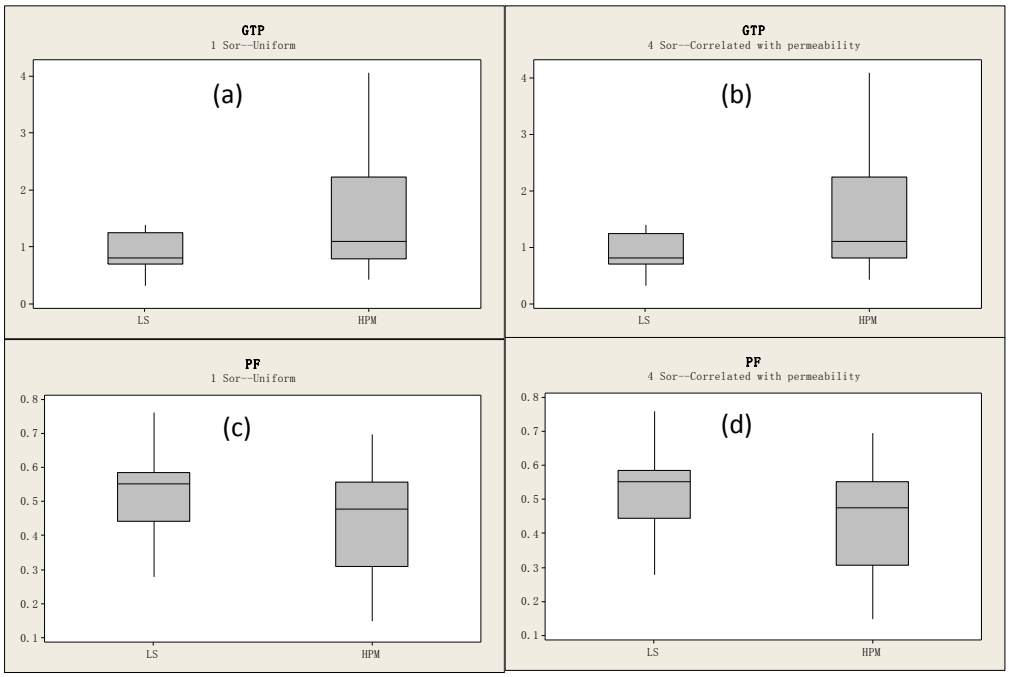

Figure 4.6 Sensitivity of GTP and PF to capillary pressure-saturation parameters with a,c) uniform residual organic saturation and b,d) residual organic saturation correlated to permeability

The results of GTP and PF for case 1 to case 4 are presented in Figure 4.6, showing the influence of capillary pressure-saturation parameters and residual organic saturations on the prediction of the ratio of ganglia to pool. With HPM the prediction for mean GTP is about 30% to 50% higher than that with Leverett scaling, and the range for GTP is about 60% larger than that with Leverett scaling. This result means that when HPM is adopted, the mass present in ganglia tends to increase, so more PCE is entrapped in the field as discrete ganglia. Accordingly, the prediction for PF tends to be 10% to 45% smaller with HPM than that with Leverett scaling. Figure 4.6 also indicates that residual organic saturation does not have a notable influence on GTP or PF.

A nonparametric test called two-sample Kolmogorov–Smirnov test (K–S test) (Fasano and Franceschini, 1987) was performed to quantify the distance between the results for selected simulation cases. In the two-sample K–S test, the null hypothesis is that the samples are drawn from the same distribution. The null hypothesis is rejected at a confidence level α if the K-S test statistic is larger than the critical value for the test (Fasano and Franceschini, 1987). In this study, the two-sample K–S test was performed by Minitab (Minitab, Inc., 2011), and the results for cases 1 to 4 are shown in Table 4.2.

Table 4.2 K-S Test Statistic for Cases 1 to 4 (Critical Value = 0.441, $\alpha = 0.05$)

	s_o^{max}	x_{cm}	z_{cm}	σ_{xx}^2	σ_{zz}^2	GTP	PF
Case 1 vs. Case 2	0.947	0.736	0.526	0.842	0.315	0.368	0.368
Case 3 vs. Case 4	0.947	0.736	0.473	0.842	0.315	0.368	0.368
Case 1 vs. Case 3	0.052	0.052	0.052	0.105	0.157	0.105	0.105
Case 2 vs. Case 4	0.105	0.105	0.105	0.105	0.052	0.105	0.105

Table 4.2 lists the values of two-sample K-S test statistic for each metric from case 1 to case 4. The values higher than the critical value at the given confidence level are highlighted, which reveal that the resulted metrics are from different underlying distributions (reject the null hypothesis) and demonstrate the influence of the related factors for the two cases tested. It can be seen from Table 4.2 that for case 1 and case 2 (or case 3 and case 4), the different sets of capillary pressure-saturation parameters (Leverett scaling for cases 1 and 3 and HPM for cases 2 and 4) resulted in different distributions of s_o^{max}, x_{cm}, z_{cm}, and σ_{xx}^2 and therefore have strong influence on the simulation of these metrics. The test between case 1 and case 3 (or case 2 and case 4) does not show any statistic value higher than the critical value (0.441), which again demonstrates that the residual organic saturation does not strongly

influence the simulation of DNAPL entrapment and infiltration.

Overall, Figures 4.3 to 4.6 and Table 4.2 reveal that the approach employed to determine the capillary pressure-saturation parameters is of critical importance in simulating DNAPL infiltration behavior. The choices determining residual organic saturation, whether correlated or not correlated with permeability, have nearly negligible influence on predicting DNAPL migration and entrapment.

4.3 Goal 2: To investigate the influence of spill rates

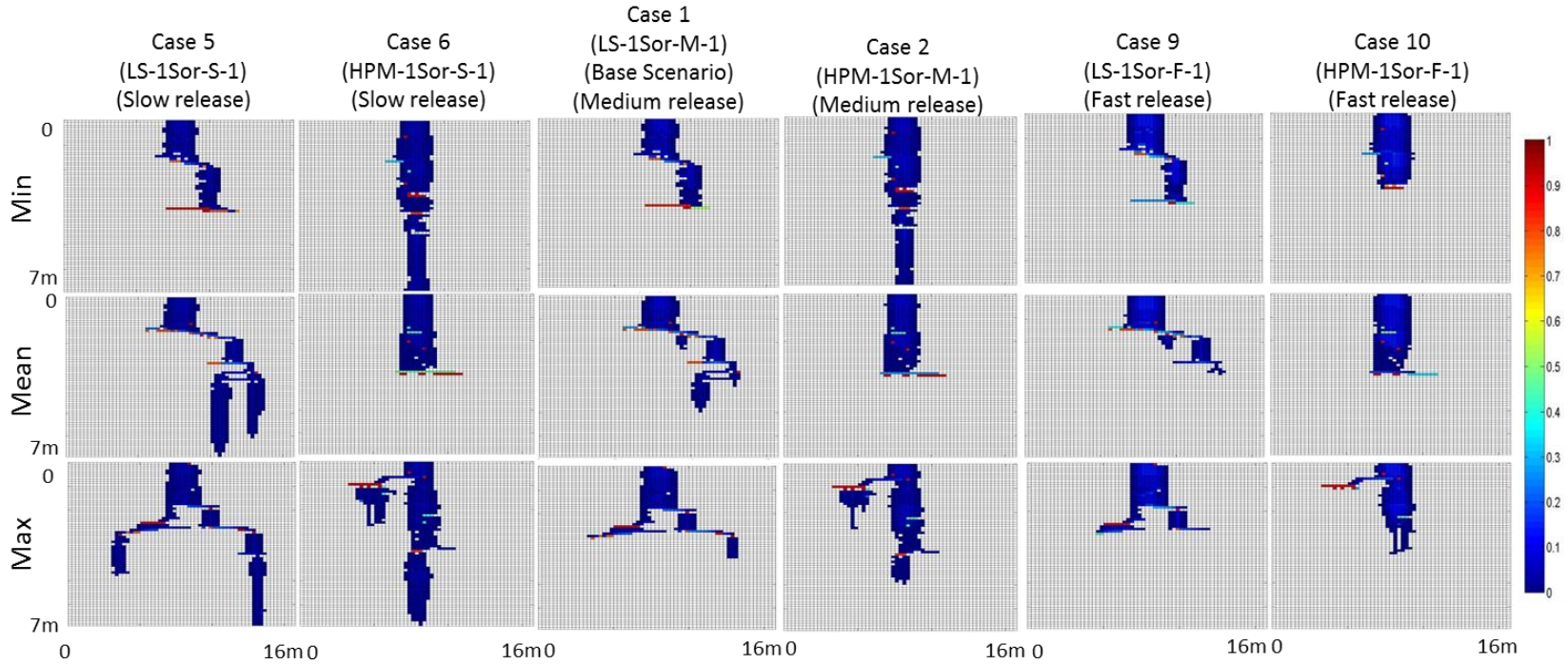

Figure 4.7 Representative PCE saturation distributions for simulation case 1, case 2, case 5, case 6, case 9 and case 10

The second goal was to explore the influence that the spill rate exerts on PCE infiltration and entrapment. This was accomplished by case 1 and 2 simulated under medium spill rate (2 L/day), case 5 and case 6 simulated under slow spill rate (0.5 L/day), and case 9 and case 10 simulated under fast spill rate (20 L/day). The combination of these six cases can be used to explore the influence of spill rate with two different sets of capillary pressure-saturation parameters.

Figure 4.7 illustrates the PCE distribution under different release rates with Leverett scaling and HPM. Here, the representative simulations for minimum, the value closest to the mean, and maximum σ_{xx}^2 from the 20 simulations for cases 1 (or case 2) were chosen at first. Then simulation results performed from the same permeability realizations for case 5 and case 9 (or case 6 and case 10) were chosen and shown in each row. Therefore, along the same row, the permeability realizations for case 1, case 5, and case 9 (or case 2, case 6, and case 10) are the same. In this way, the pathways for PCE are similar within the same realizations and, the results are more comparable.

From Figure 4.7, a clear decrease of penetration depth can be observed with increasing spill rate. For the same realization and capillary pressure model, high saturation pools occur at similar locations. With increasing spill rate, both the horizontal and vertical spread are reduced; the PCE tends to be trapped in a smaller region with higher average saturation values in each cell.

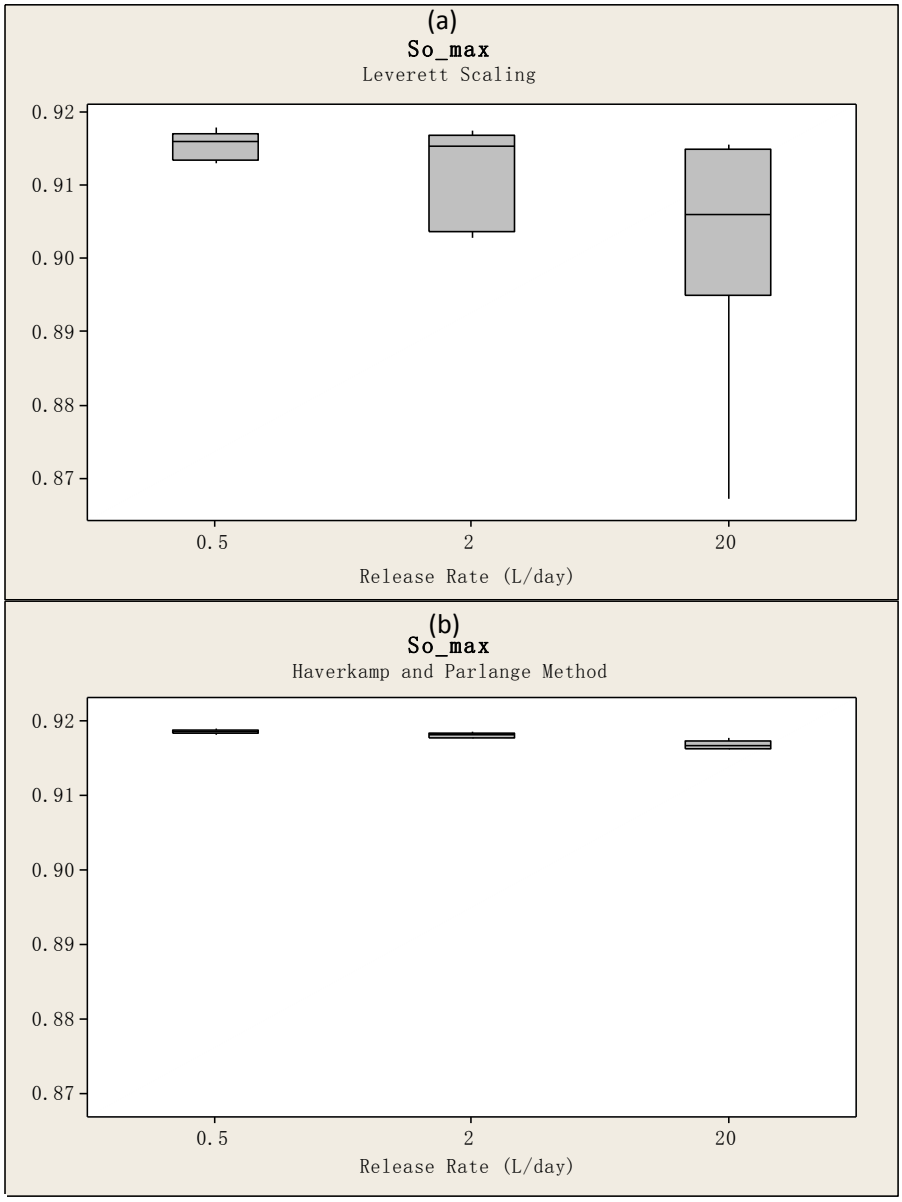

Figure 4.8 Sensitivity of s_o^{max} to spill rates with a) Leverett scaling and b) HPM

Figure 4.8 explores the effects of spill rate on PCE distribution with Leverett scaling and HPM. s_o^{max} exhibits a reducing trend with increasing spill rate in this highly heterogeneous aquifer. With Leverett scaling, the mean value of s_o^{max} tends to reduce 0.5% to 1.5% with increasing release rate. When using HPM, the mean s_o^{max} with the slow release rate is about 0.05% to 3% higher than that with fast release rate. Although the reducing trend with increasing spill rate can be observed with both sets of capillary pressure-saturation

parameters, the predictions for the mean s_o^{max} are similar. However, a 30% to 60% increase for the range of s_o^{max} with increasing spill rate can be observed when Leverett scaling is adopted, which demonstrates the influence of spill rate on s_o^{max} variability.

Dekker and Abriola (2000) reported that with increasing spill rate, the values for s_o^{max} would increase in mildly heterogeneous aquifer, which is contrary to the results for s_o^{max} in this study. But they studied the interplay of permeability with spill rate and found that the increase of heterogeneity would obscure the effects of spill rate on the DNAPL migration. Thus for our highly heterogeneous permeability field, the influence of spill rate on s_o^{max} is noticeable compared to that of mildly heterogeneous aquifers.

For further exploration, another metric, the values of overall average organic saturation ($\bar{s_o}$), was calculated for the six cases studied for goal 2. Figure 4.9 shows the boxplot for $\bar{s_o}$ under slow, medium, and fast release rates with either Leverett scaling or HPM. With Leverett scaling, the mean ensemble values of $\bar{s_o}$ are 6.01×10^{-2}, 6.51×10^{-2}, and 8.65×10^{-2}, respectively for slow, medium, and fast release. With HPM, the mean ensemble values of $\bar{s_o}$ are 4.42×10^{-2}, 5.03×10^{-2}, and 6.72×10^{-2}, respectively for slow, medium, and fast release. A clear increasing trend of $\bar{s_o}$ with increasing spill rate can be found in Figure 4.9, with both sets of capillary pressure-saturation parameters. An approximately 10% to 25% increase of $\bar{s_o}$ can be observed with both Leverett scaling and HPM.

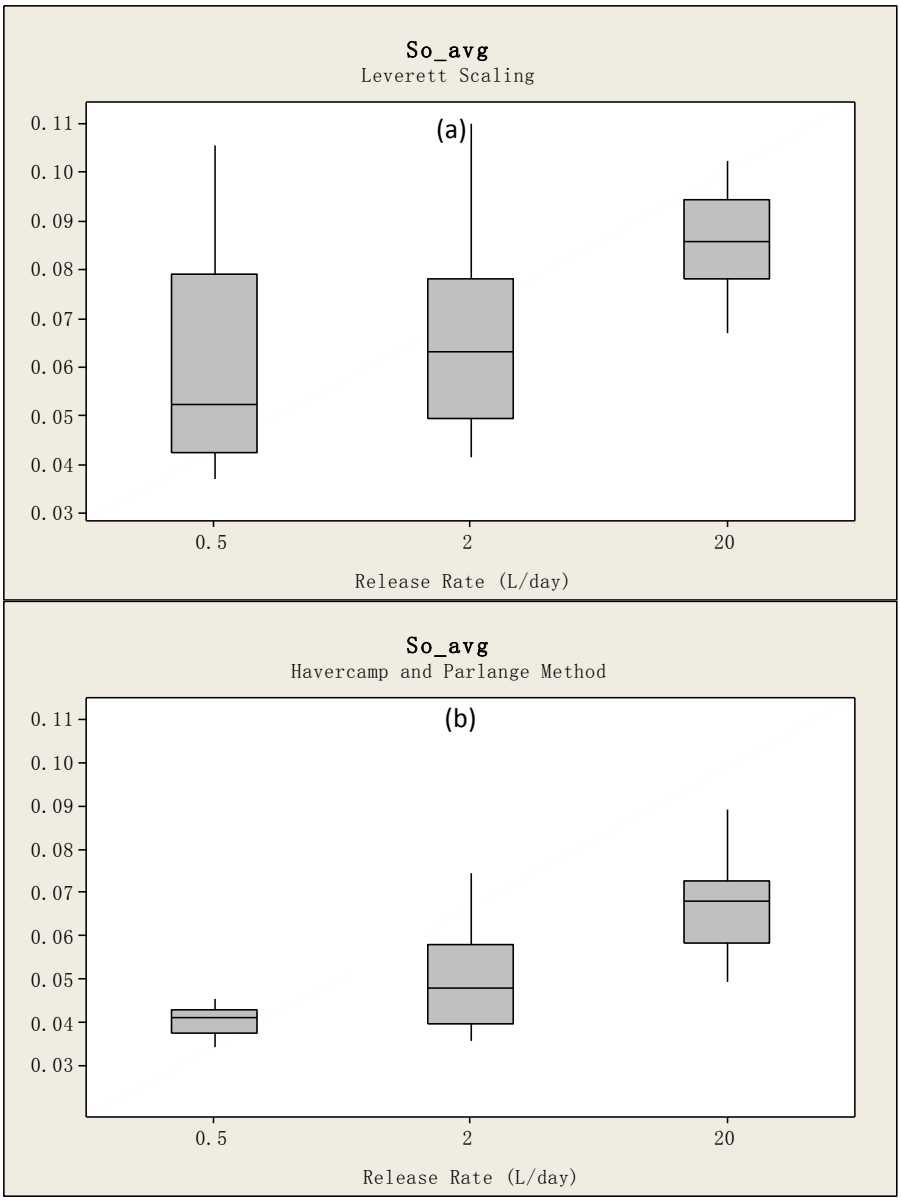

Figure 4.9 Sensitivity of $\bar{s_o}$ to spill rates with a) Leverett scaling and b) HPM

Therefore, despite the decreasing trend of s_o^{max} with increasing spill rate, the average $\bar{s_o}$ tends to increase with spill rate in the highly heterogeneous aquifer.

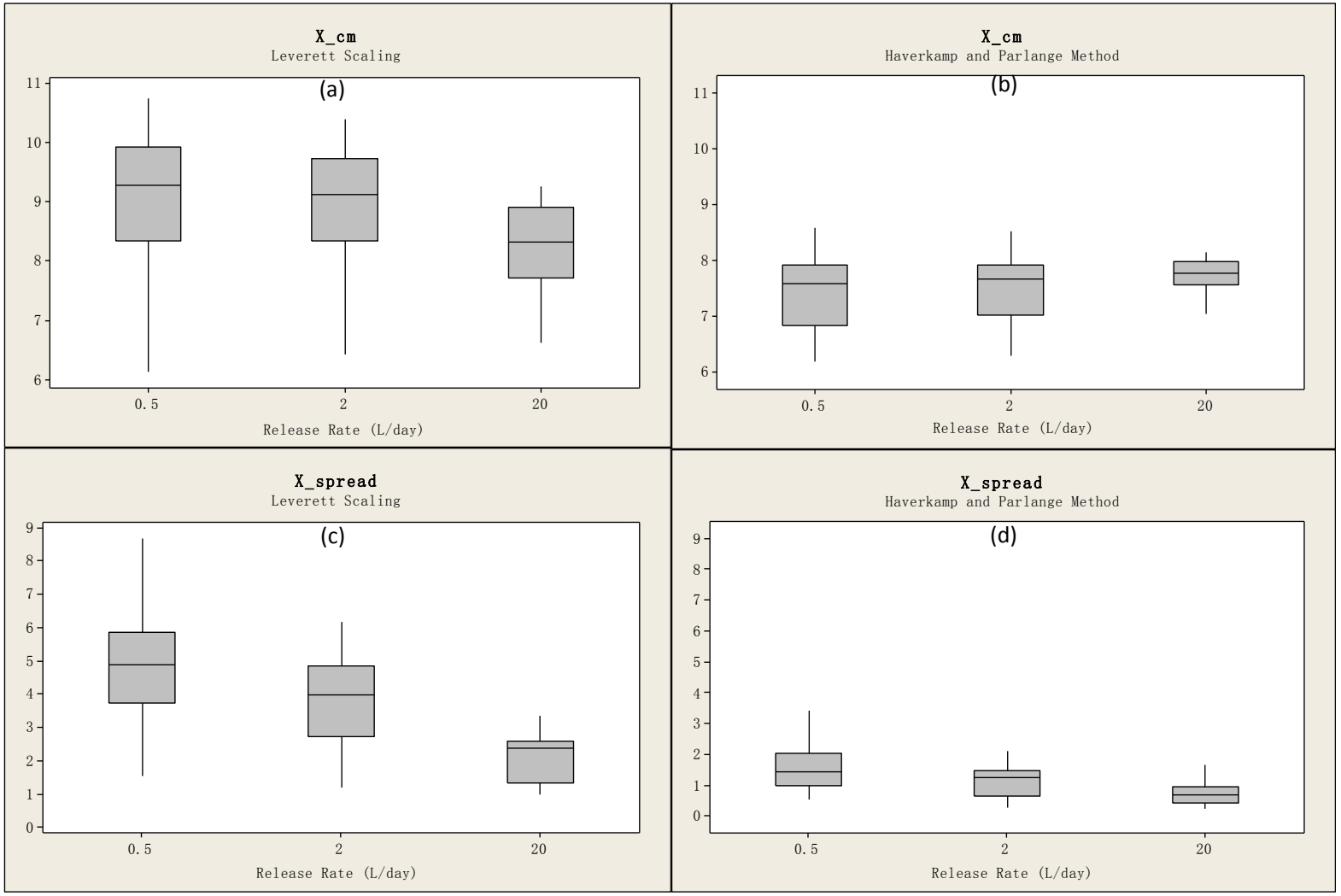

Figure 4.10 Sensitivity of x_{cm} and σ_{xx}^2 to spill rates with a, c) Leverett scaling and b,d) HPM

Figure 4.10 presents the changes in horizontal center of mass (x_{cm}) of PCE distribution with increasing spill rates. When using Leveret scaling, the mean value and range for x_{cm} tends to decrease with increasing spill rate. However, with HPM, the changes for the mean x_{cm} with spill rates follow an opposite trend. It is worth noting that with both sets of capillary pressure-saturation parameters, x_{cm} approaches 8 m (center of the 2-D domain along horizontal direction) with a faster spill rate. In addition, for the range of x_{cm}, there is a 25% to 45% decrease with Leverett scaling and a 10% to 40% decrease with HPM as the spill rate increases. These results reveal that PCE is more likely to be constrained in the horizontal center with increasing spill rate.

Figure 4.10 (c) and Figure 4.10 (d) depict the PCE horizontal spread (σ_{xx}^2) under different spill rates with Leveret scaling and HPM. The mean value for σ_{xx}^2 under slow release tend to be approximately 20% to 30% higher than that under medium release and, about 50% to 60% higher than that under fast release rate, with both sets of capillary pressure-saturation parameters. These results demonstrate the strong influence of spill rate on the extent of horizontal spread for PCE.

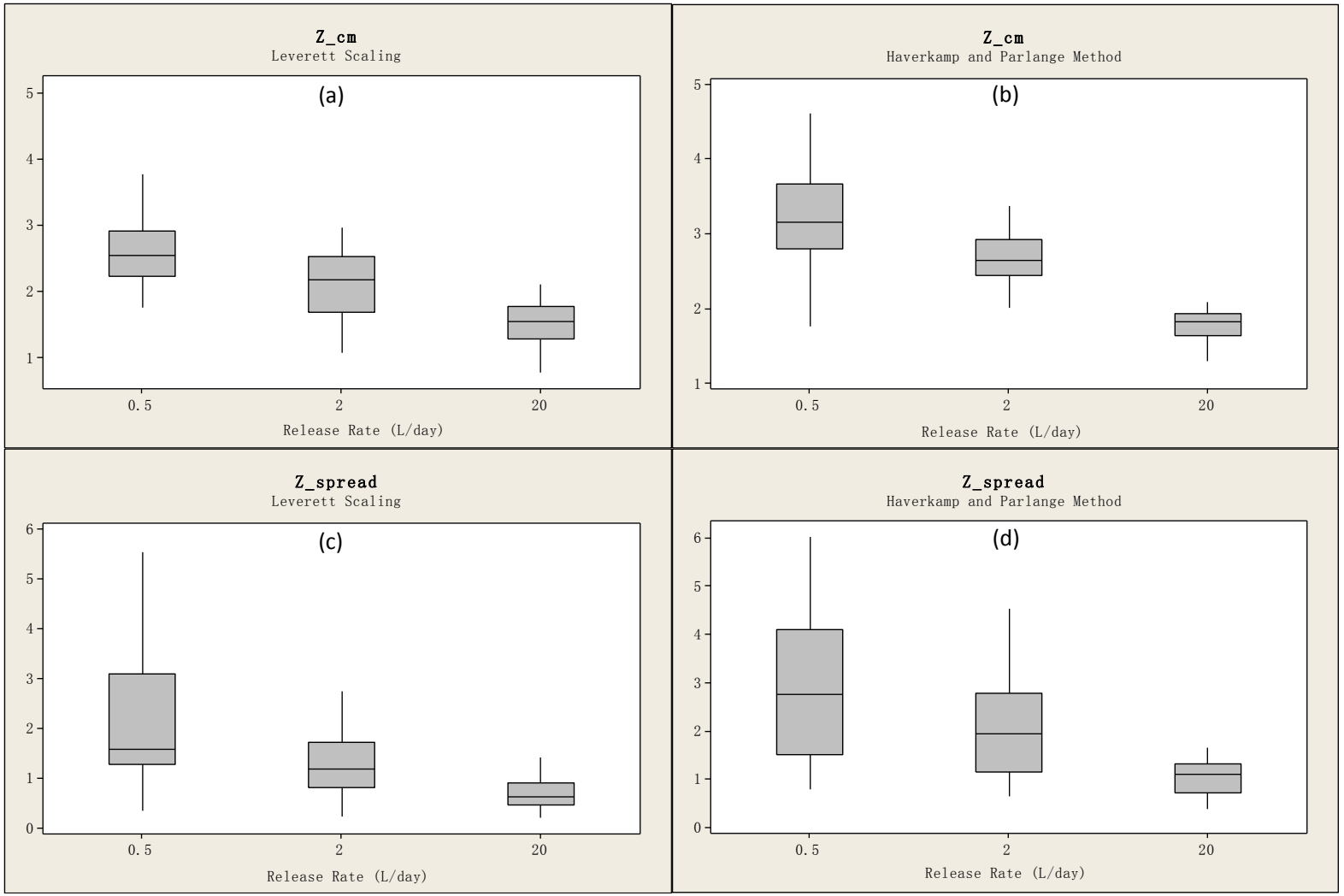

Figure 4.11 Sensitivity of z_{cm} and σ_{zz}^2 to spill rates with a, c) Leverett scaling and b,d) HPM

Figure 4.11 reveals a reducing trend for z_{cm} and σ_{zz}^2 with increasing spill rates. Statistical analysis indicates an approximately 20% to 45% decrease for the mean penetration depth of PCE with increasing spill rate for both sets of capillary pressure-saturation parameters. The range of z_{cm} shows a 10% to 40% decrease with Leverett scaling and a 25% to 65% decrease with HPM. These results reveal that with increasing spill rate, PCE tends to be trapped mainly in the upper regions and can hardly overcome the capillary entry pressure forces to migrate vertically.

Similarly, a 30% to 70% decrease for mean σ_{zz}^2 can be found with increasing spill rate for both sets of capillary pressure-saturation parameters. Also, a clear trend of reducing variance of σ_{zz}^2 with increasing spill rate can be observed in Figure 4.11 (c) and (d) with either Leverett scaling or HPM. The results for z_{cm} and σ_{zz}^2 reveal the strong influence of spill rate on PCE infiltration behavior in the vertical direction.

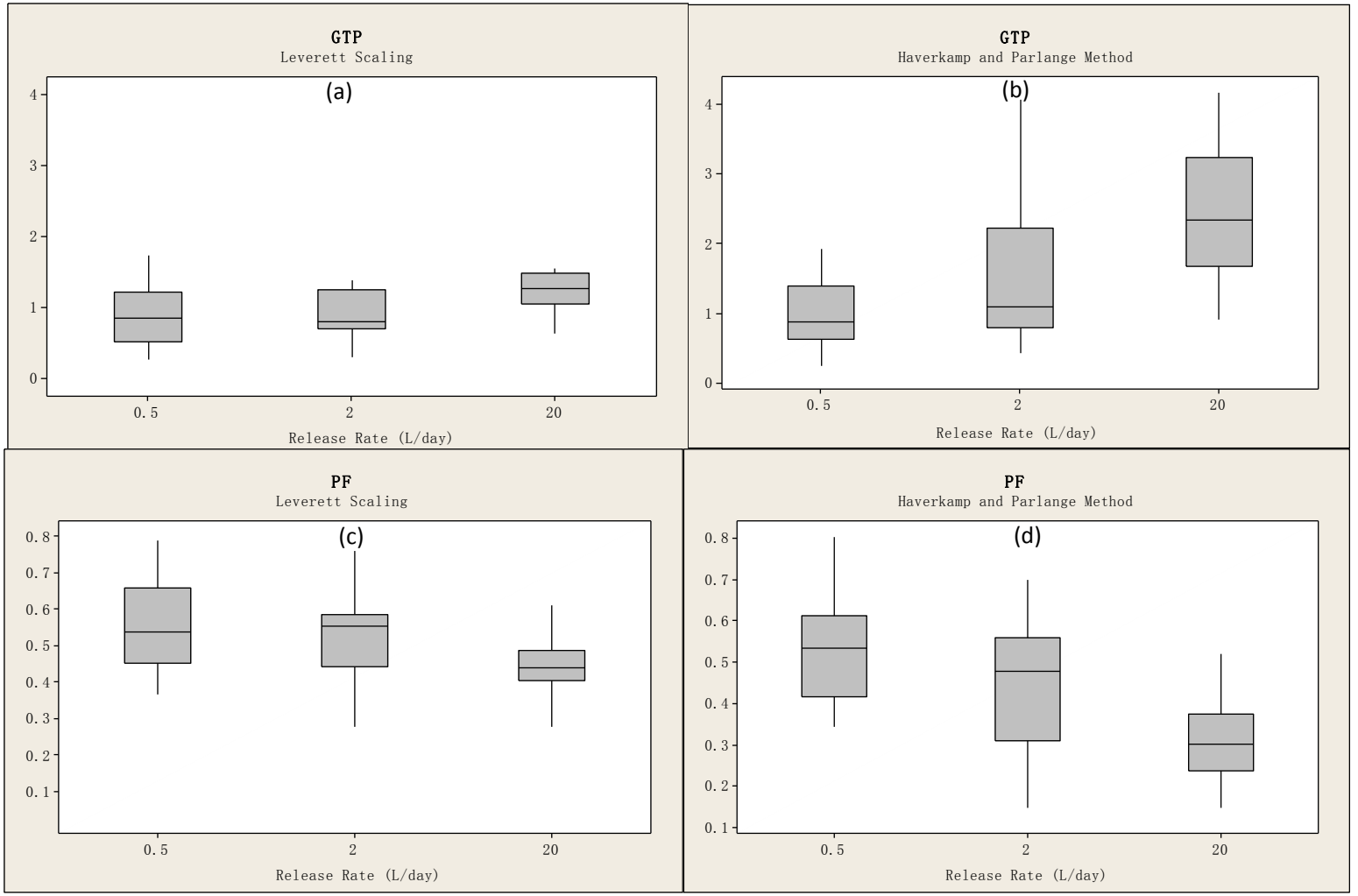

Figure 4.12 Sensitivity of GTP and PF to spill rates with a, c) Leverett scaling and b,d) HPM

Figure 4.12 illustrates the effects of spill rate on GTP and PF for PCE distributions. The results show that with Leverett scaling, the GTP values obtained from slow and medium release are close (the mean GTP for medium release is about 10% higher than that for slow release). But under fast release, the GTP increases markedly (about 30% higher than medium release). Correspondingly, although there is a trend of reducing PF with increasing spill rate, the mean PF obtained from slow and medium release are similar (the PF for medium release is only about 5% smaller than that for slow release). When the HPM is used, the increasing trend of GTP and decreasing trend of PF with larger spill rates is more obvious than those with Leverett scaling (there is a 35% to 40% increase in GTP and a 15% to 30% decrease in PF with increasing release rate).

One explanation for the increasing trend of GTP with increasing spill rate is that due to the high value of the residual organic saturation (0.235) in this study, there might be a smaller number of cells that contain PCE saturation values higher than the maximum residual organic saturation (s_{or}^{max}) with increasing release rate. This s_{or}^{max}, which is for the background lithofacies (Gcm), defines the threshold for ganglia and pool. For the studies in mildly heterogeneous aquifers, the s_{or}^{max} is much smaller than 0.235 (usually about 0.15). The relatively high s_{or}^{max} in this study is associated with two factors: (1) there was no drainage curve reported and no reported value of s_{or}^{max} for Herten site, thus it was difficult to estimate the value of s_{or}^{max}; (2) in order to make this work comparable to Dekker and Abriola (2000) in mildly heterogeneous aquifers, the same correlation (Hoag and Marley (1986)) was used here. The use of this correlation is also supported by the fact that the

range of permeability given by Hoag and Marley (1986) overlaps with the majority of the range of permeability for the Herten site.

Table 4.3 K-S Test Statistic for Cases 1, 2, 5, 6, 9, and 10 (Critical Value = 0.435, α = 0.05)

	s_o^{max}	$\overline{s_o}$	x_{cm}	z_{cm}	σ_{xx}^2	σ_{zz}^2	GTP	PF
Case 1 vs. Case 5	0.331	0.281	0.184	0.431	0.289	0.434	0.194	0.194
Case 1 vs. Case 9	0.481	0.584	0.426	0.536	0.634	0.492	0.484	0.484
Case 5 vs. Case 9	0.7	0.65	0.5	0.8	0.8	0.75	0.5	0.5
Case 2 vs. Case 6	0.423	0.431	0.142	0.486	0.321	0.294	0.315	0.315
Case 2 vs. Case 10	0.894	0.634	0.271	0.842	0.428	0.581	0.534	0.534
Case 6 vs. Case 10	0.95	0.85	0.3	0.9	0.6	0.75	0.65	0.65

Table 4.3 shows that with Leverett scaling, all the resulted metrics under slow and medium release do not have different underline distributions, but with increasing spill rate, more metrics tend to have different underline distributions. Similarly, with HPM, more metrics tend to have different underline distributions with increasing spill rate, and only x_{cm} does not reveal clear effects of spill rate. The results shown in Table 4.3 agree with those in Figure 4.8 to Figure 4.12. Therefore, the strong influence of spill rate on every metric can be demonstrated.

4.4 Goal 3: To investigate the effects of hypothetical field structures

The focus of goal 3 is placed on the examination of the influence of hypothetical permeability field structure on the DNAPL migration. For this, simulation results for case 1, case 2, case 7 and case 8 are compared to explore the infiltration and entrapment behavior in different field formations. Case 1 and case 2 are simulated in hypothetical permeability field 1, and case 7 and case 8 are simulated in hypothetical permeability field 2. Other simulation conditions, like the release rate (2 L/day), and the total volume released into the subsurface are exactly the same. As mentioned in previous sections, the volumetric portions for each lithofacies are consistent in field 1 and 2, but the locations of low permeability layers are different. In field 1, a large low permeability layer was present on the top boundary where the PCE was released, while in field 2, no such low permeability layer was present around the release location.

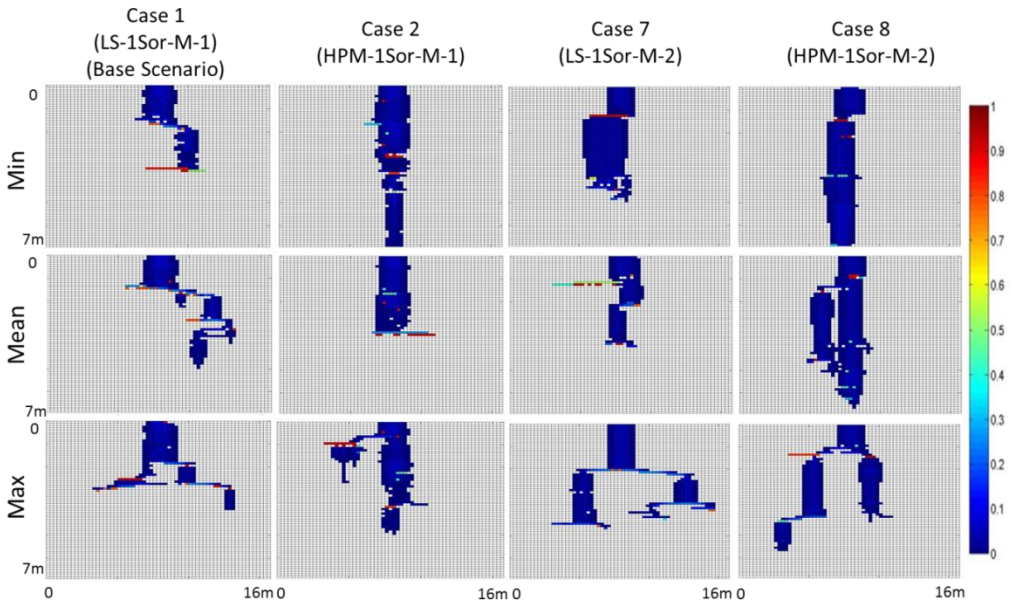

Figure 4.13 Representative PCE saturation distributions for simulation case 1, case 2, case7, and case 8

Similar with Figure 4.2 and Figure 4.7, Figure 4.13 depicts representative simulations for the minimum, value closest to mean, and maximum σ_{xx}^2 for case 1, case 2, case 7, and case 8. As Figure 4.13 shows, the representative source zones for field 1 and field 2 display entirely different pathways. The different field structure realizations greatly changed the regions where PCE pools.

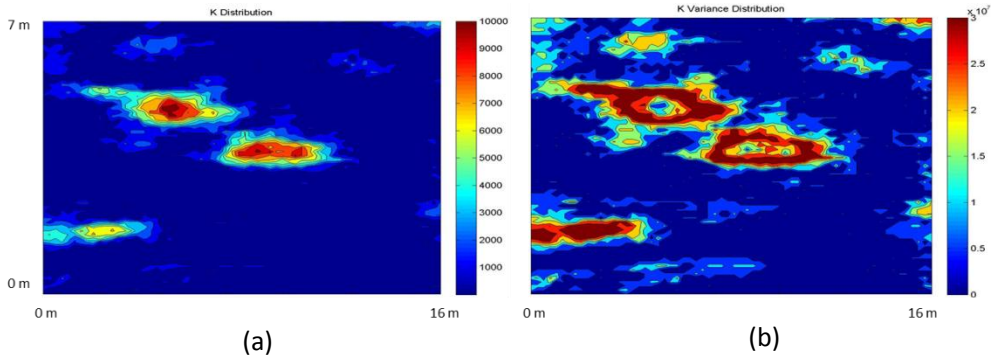

Figure 4.14 a) Mean and b) Variance for hydraulic conductivity K (m/d) by pixel for field 1

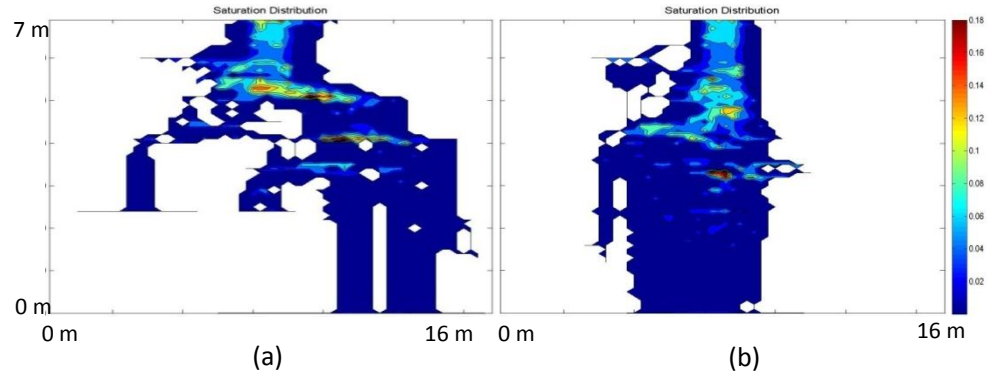

Figure 4.15 Average saturation over 20 realizations by pixel for a) case 1 and b) case 2 within field 1

Figure 4.14 depicts the mean and variance for the hydraulic conductivity K (m/d) over the 20 permeability realizations for hypothetical field 1, which are obtained by calculating through every pixel (on the same coordinate position). Figure 4.15 depicts the average PCE saturation for every pixel at the same

location over the 20 permeability realizations for field 1 with either Leverett scaling or HPM. Inspecting Figure 4.14 and 4.15, it can be inferred that high saturation values tend to occur above the areas with high hydraulic conductivity or high variance of hydraulic conductivity. It is possible that the saturation is correlated with the value or the variance of hydraulic conductivity.

Figure 4.16 and Figure 4.17 present the same trend as Figure 4.14 and Figure 4.15 for hypothetical field 2. In field 2, the high mean value and variance of K are present at lower regions. High saturation values in field 2 tend to occur at lower regions.

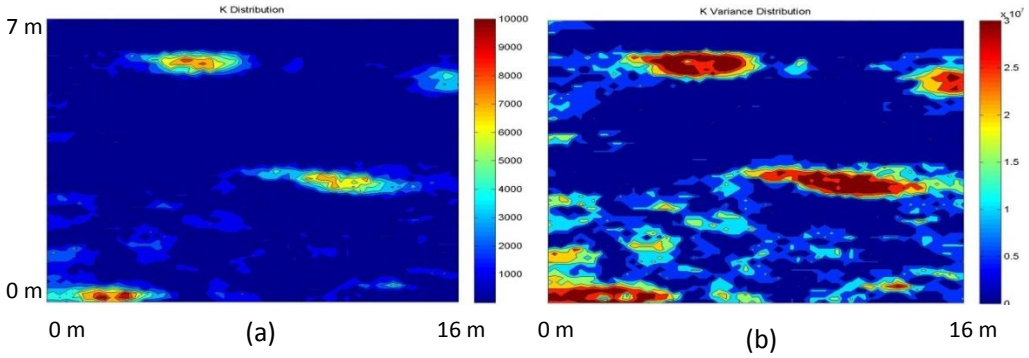

Figure 4.16 a) Mean and b) Variance for hydraulic conductivity K (m/d) by pixel for field 2

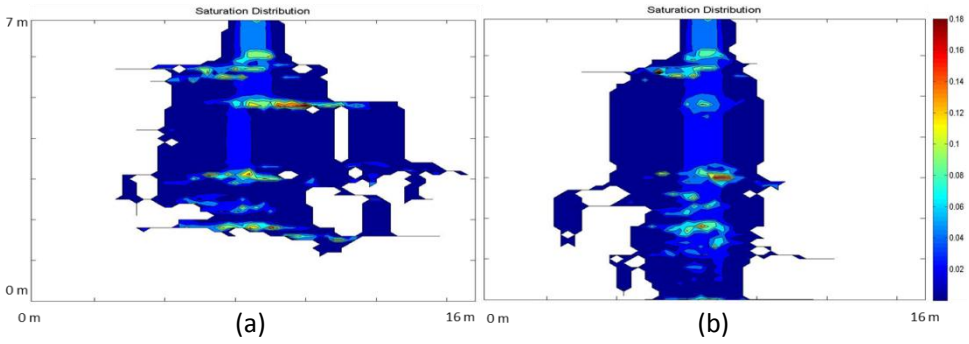

Figure 4.17 Average saturation over 20 realizations by pixel for a) case 7 and b) case 8 within field 2

The Pearson correlation coefficient was calculated for K and the organic saturation (s_o) shown in Figure 4.14 to Figure 4.17. For field 1, the correlation coefficient between the average of K and average of s_o is 0.041 with Leverett scaling and 0.199 with HPM. The correlation coefficient between the variance of K and variance of s_o is 0.025 with Leverett scaling and 0.216 with HPM. For field 2, the correlation coefficient between average of K and s_o is 0.076 with Leverett scaling and 0.108 with HPM, while the correlation coefficient between the variance of K and s_o is 0.081 with Leverett scaling and 0.131 with HPM. The values of correlation coefficients for K and s_o are small in field 1 and 2 with both sets of capillary pressure-saturation parameters, which indicate that there is no statistically significant correlation of s_o to the average or the variance of K.

To test the influence of hypothetical field structure, detailed descriptions and discussions for each metric are given in Figure 4.18 to Figure 4.21.

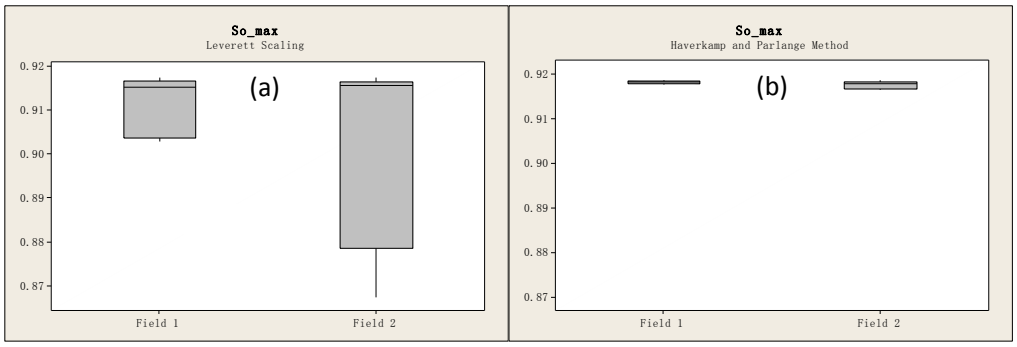

Figure 4.18 Sensitivity of s_o^{max} to hypothetical field formation with a) Leverett scalingand b) HPM

Figure 4.18 shows the mean and range for s_o^{max} in field 1 and field 2 with either Leverett scaling or HPM. The boxplot suggests that for field 2 where the capillary barriers are not present on the top boundaries, the range of s_o^{max} is

greater than that for field 1 with Leverett scaling. But the median for s_o^{max} with both sets of capillary pressure-saturation parameters and the range for s_o^{max} with HPM are similar in field 1 and field 2. As a result, for the control of s_o^{max}, the hypothetical field structure has a relatively small influence.

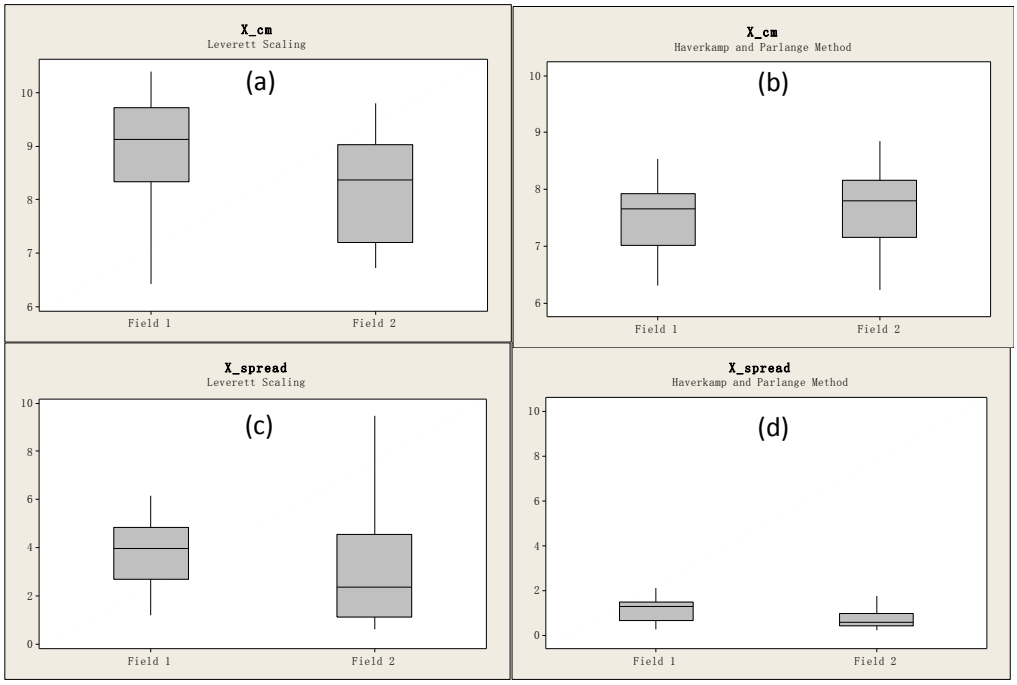

Figure 4.19 Sensitivity of x_{cm} and σ_{xx}^2 to hypothetical field formation with a, c) Leverett scaling and b,d) HPM

Figure 4.19 shows the predictions of x_{cm} and σ_{xx}^2 for field 1 and field 2 with Leverett scaling and HPM. With Leverett scaling, the mean value of x_{cm} for field 1 is about 6% larger than that for field 2, while with HPM the mean value of x_{cm} for field 1 is about 3.5% smaller than that for field 2. The difference of x_{cm} for field 1 and 2 is not significant, but for field 2 the center of PCE mass is closer to the horizontal center of the domain.

Figure 4.19 (c) and (d) show that with Leverett scaling and HPM the influence of permeability field structure on σ_{xx}^2 is different. With both Leverett scaling and HPM, the mean σ_{xx}^2 is about 20% larger in field 1 than in field 2 and, the

range of σ_{xx}^2 is about 30% to 40% higher in field 2 than in field 1. Therefore, although the field structure does not have significant influence on the prediction of x_{cm}, it has a relatively high influence on σ_{xx}^2, regardless of the set of capillary pressure-saturation parameters employed.

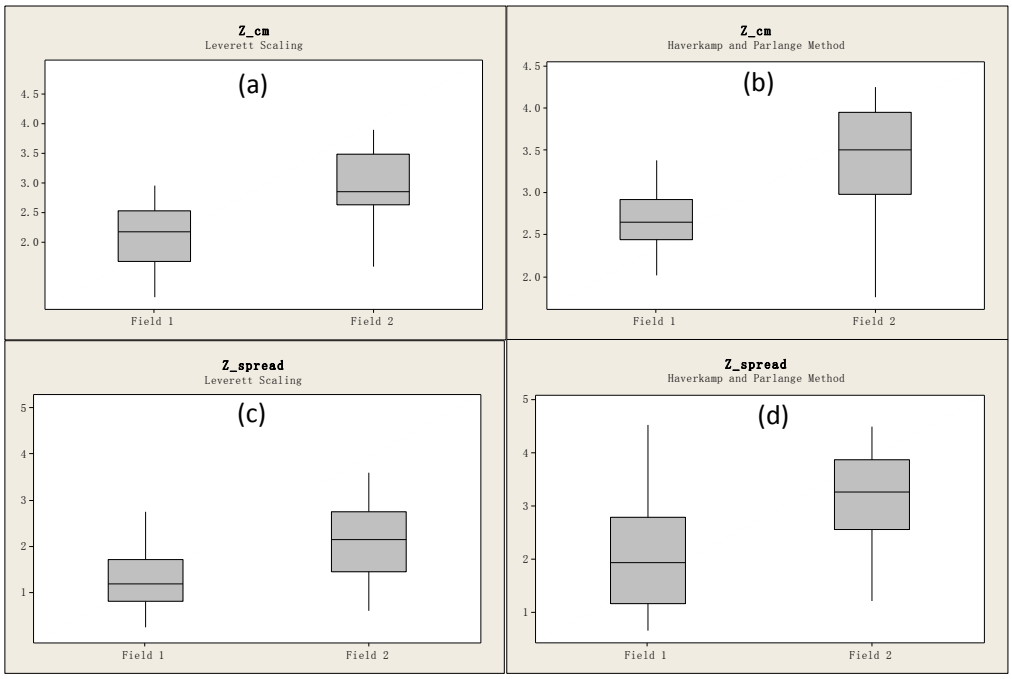

Figure 4.20 Sensitivity of z_{cm} and σ_{zz}^2 to hypothetical field formation with a, c) Leverett scaling and b,d) HPM

Figure 4.20 describes the PCE vertical penetration (z_{cm}) and spread (σ_{zz}^2) in field 1 and field 2 with Leverett scaling and HPM. To a large extent the hypothetical field structure influences the vertical migration of PCE. In field 2 where the large capillary barrier is present at a deeper location, z_{cm} tends to be approximately 20% to 30% higher than that for field 1, and the σ_{zz}^2 is about 20% to 30% greater than that for field 2, with both sets of capillary pressure-saturation parameters. Apparently, in field 2 the PCE tends to migrate deeper into the subsurface. Therefore, the location of capillary barriers needs to be carefully taken into consideration when simulating PCE subsurface

entrapment and infiltration behavior in highly heterogeneous permeability fields.

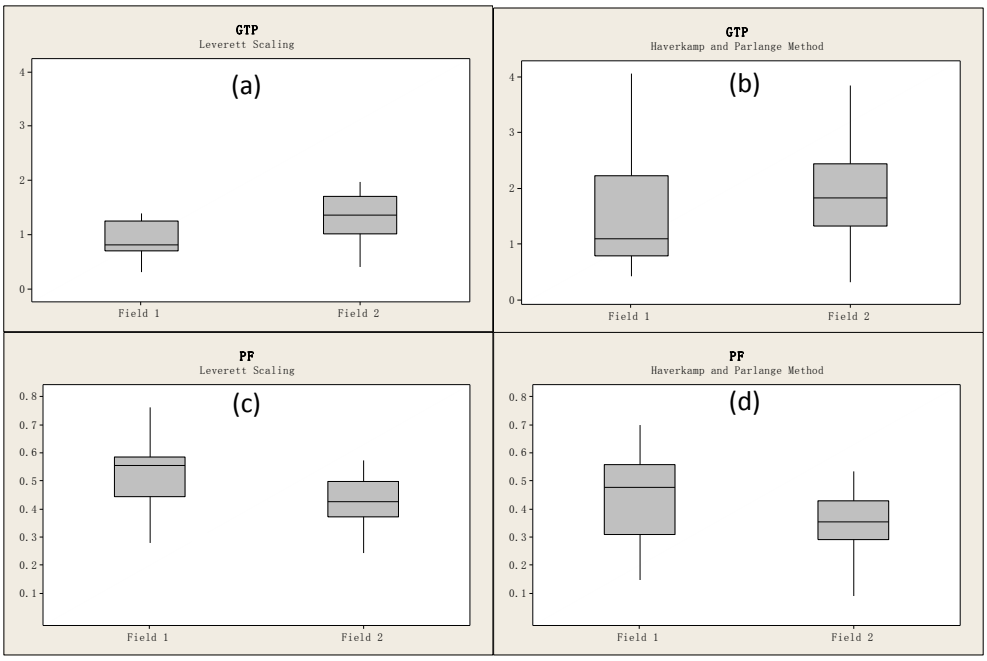

Figure 4.21 Sensitivity of GTP and PF to hypothetical field formation with a, c) Leverett scaling and b,d) HPM

The sensitivity of GTP and PF to the field structures with both Leverett scaling and HPM are summarized in Figure 4.21. In general, the mean GTP values in field 2 are about 30% higher than those in field 1. Correspondingly, the mean PF values tend to be about 20% smaller in field 2. The smaller extent of pooling in field 2 is attributed to a large amount of PCE entrapped as ganglia in the top areas of field 2 where capillary barriers are not present. As a result, when the PCE reaches the capillary barrier located at the bottom of the domain, a smaller volume of free PCE accumulates above it. On the contrary, PCE accumulates around the release areas of field 1. Consequently, a higher amount of ganglia regions occurred in field 2 and mass present in ganglia regions is greater in this field.

Table 4.4 K-S Test Statistic for Cases 1, 2, 7, and 8 (Critical Value = 0.435, α = 0.05)

	s_o^{max}	x_{cm}	z_{cm}	σ_{xx}^2	σ_{zz}^2	GTP	PF
Case 1 vs. Case 7	0.178	0.347	0.744	0.394	0.486	0.534	0.534
Case 2 vs. Case 8	0.397	0.244	0.594	0.436	0.484	0.531	0.531

Results from the two-sample K-S test show that with Leverett scaling, the metrics z_{cm}, σ_{zz}^2, GTP, and PF tend to have different underline distribution in field 1 and field 2. With HPM, another metric σ_{xx}^2, together these same four metrics with Leverett scaling, reveal quantifiable differences in field 1 and field 2.

In general, five out of the seven studied metrics in this work are sensitive to the changes of location of low permeability layers present in the field, namely σ_{xx}^2, z_{cm}, σ_{zz}^2, GTP, and PF. The clear discrepancy of these metrics between field 1 and field 2 proves that the location of the low permeability layer with extensive horizontal correlation length is of great importance in simulating DNAPL entrapment and infiltration behavior. The geostatistical simulation of extensive horizontal layers is successful with the TP/MC. Therefore, the TP/MC approach has to be carefully design when generating the hypothetical field realizations.

4.5 Goal 4: To compare 2-D and 3-D simulation results

To accomplish goal 4, to briefly investigate the ability to extend the conclusions based on 2-D simulations to 3-D simulations in highly heterogeneous permeability fields, 3-D simulations were performed using the University of Texas Chemical Compositional Simulator (UTCHEM) (Delshad et al., 1996). Since the 3-D simulations are CPU time consuming (in general one simulation takes two to three days), it is impossible to run the 3-D simulations for the whole ensemble of 20 realizations for all the ten cases due to the time limit of this study. Therefore, to obtain insight into PCE entrapment and infiltration behavior in 3-D, only 1 of the 20 realizations was chosen and simulated under the simulation cases: 1, 2, 5, 6, 9, and 10. These six cases include Leverett scaling and HPM under slow, medium, and fast release rates, thus the influence of capillary pressure-saturation parameters and the spill rates on 3-D simulation of PCE migration can be briefly examined.

Figure 4.22 illustrates the source areas where the PCE was released. For the 3-D permeability field realization, a total volume of 320 L of PCE was released from a 5×4 nodal area. On the top of the 2-D cross section that corresponds to the 2-D permeability field, an identical amount (80L) of PCE as the 2-D simulation was released from the center 4 nodes.

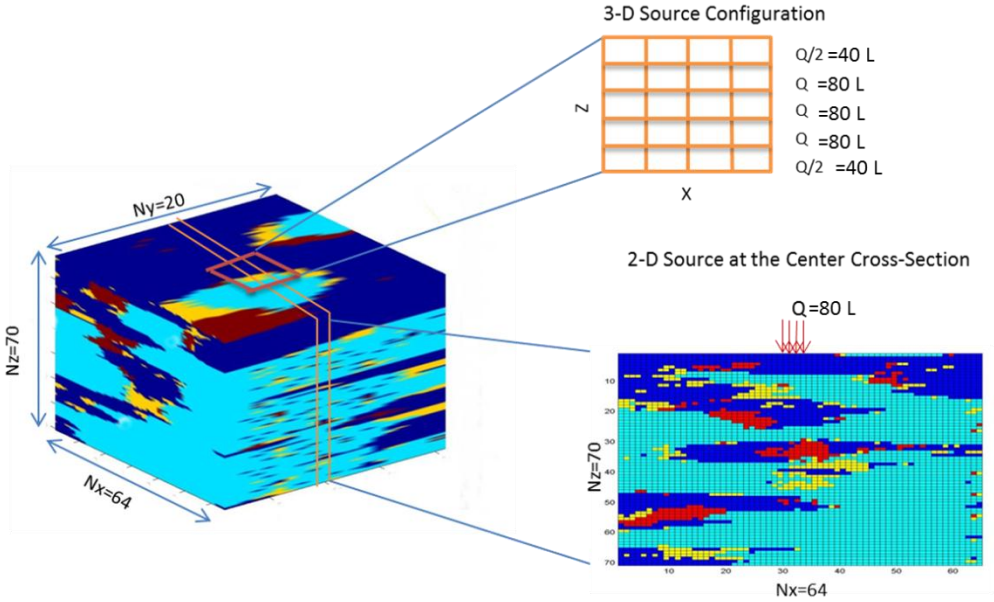

Figure 4.22 Conceptualization for the source areas of 3-D and 2-D permeability fields

To make the 2-D and 3-D simulation results comparable, the 3-D DNAPL infiltration results were sliced and the center x-z cross sections corresponding to the 2-D permeability field realizations were extracted, the resulted metric calculated from this cross section is called "2-D in 3-D" results, as shown in Figure 4.23.

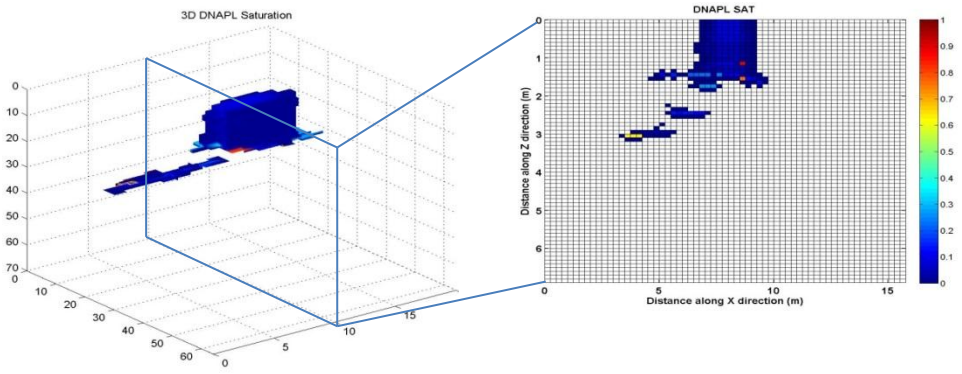

Figure 4.23 2-D simulation results extracted from 3-D simulation

Figure 4.24 depicts the PCE migration pathways for 2-D and 3-D simulations under slow, medium, and fast spill rates, with Leverett scaling. Clearly,

although the same amount of PCE is released at the same rates in identical permeability fields, 2-D and 3-D simulation results are quite different.

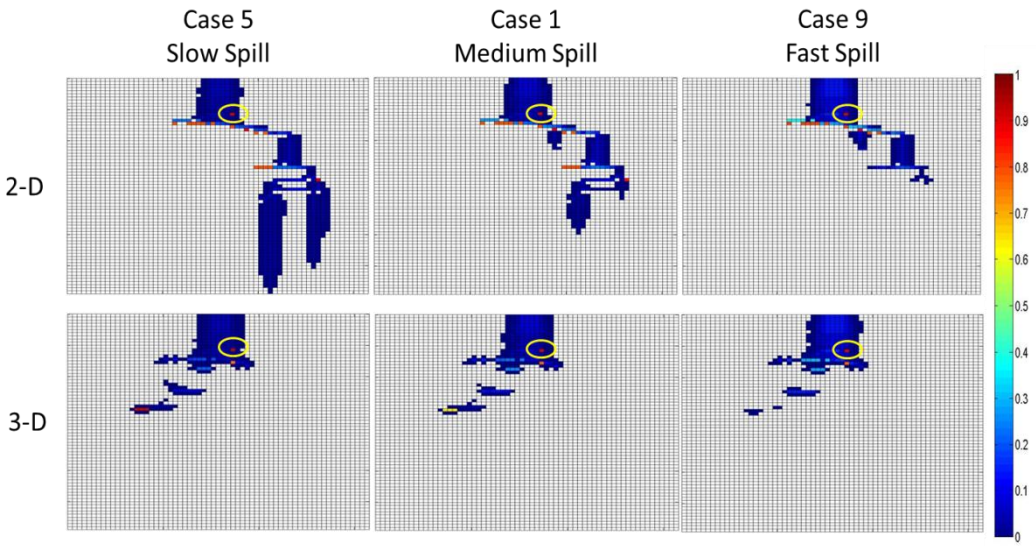

Figure 4.24 2-D and 3-D PCE saturation distribution with Leverett scaling

The different DNAPL architecture resulting from 3-D and 2-D simulations may be explained by the fact that in the 3-D domain, PCE encountering the horizontal capillary barrier moves to adjacent cross sections, whereas in the 2-D domain the adjacent cross sections do not exist. The PCE pathways for the 2-D cross sections of the 3-D simulations are not continuous, but the 3-D simulations have pathways in other planes for the PCE to continue its vertical migration. For both 2-D and 3-D simulations, there is a cell at the same location close to the release points that contains the high saturation value, as highlighted in Figure 4.24 with circles.

A strong influence of the spill rates on the PCE pathway can be observed for 2-D simulations, while for 3-D simulations, the influence of spill rates is not very clear.

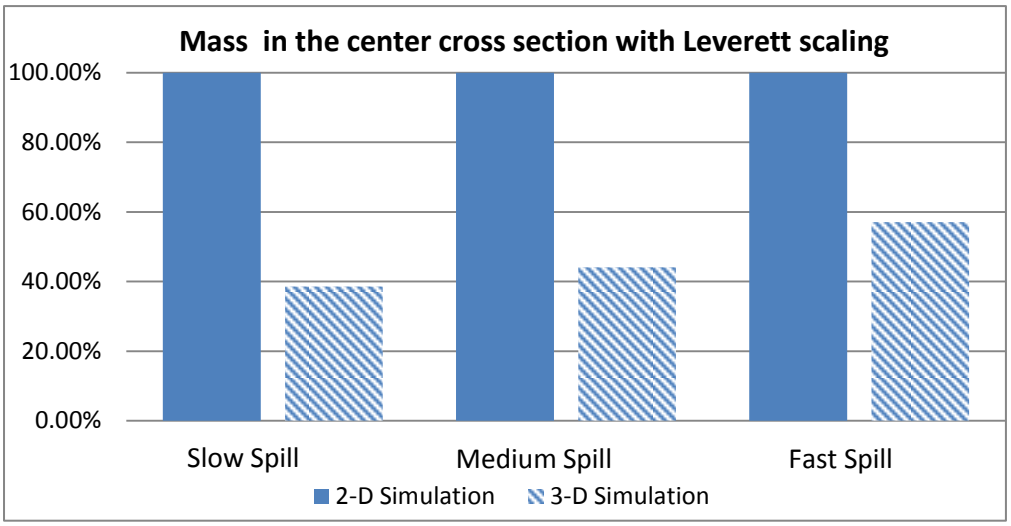

Figure 4.25 Percentage of mass in the center cross section with Leverett scaling

Since the PCE penetrates through adjacent planes in 3-D simulations, it is necessary to investigate the mass in the center cross section at the end of the simulation. Figure 4.25 is a bar diagram which investigates the percentage of mass left in the center cross section for 2-D and 3-D simulations with Leverett scaling. As mentioned previously, identical amounts of PCE mass are released into the center cross section for 2-D and 3-D simulations. According to Figure 4.25, a considerable portion of PCE moved to adjacent planes for the 3-D simulation and the amount of PCE mass left in the center cross section increases with increasing spill rates. The mass left in the center cross section is less than 40% and 45% with slow (0.5 L/day) and medium (2 L/day) release rates, but with a dramatic release rate (20 L/day) there is a noticeable increase in which the mass left in the center cross section exceeds 55%.

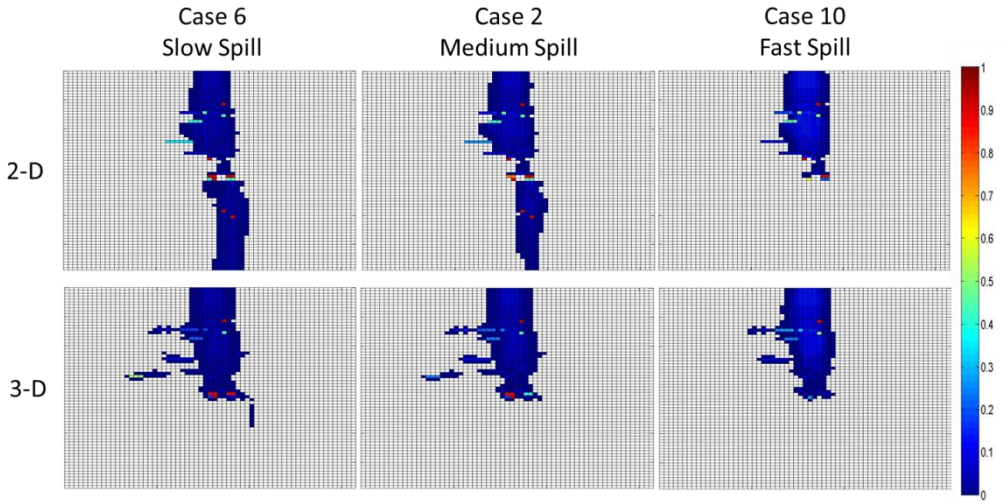

Figure 4.26 2-D and 3-D PCE saturation distribution with HPM

Figure 4.26 depicts PCE pathways for 2-D and 3-D simulations with HPM. Clearly the capillary pressure-saturation parameters strongly influence the PCE migration for both 2-D and 3-D simulations, since the PCE migration pathways are different with Leverett scaling and HPM. With HPM the pathway for PCE tends to be more continuous in the 3-D simulation than that with Leverett scaling. But there are also discontinuous pathways which indicate PCE movement to adjacent planes.

In agreement with Leverett scaling, the spill rate does not show as strong influence on the penetration depth as of 2-D simulations for 3-D simulations with HPM. But clearly with increasing spill rate, fewer pools occur at lower regions of the 2-D permeability fields.

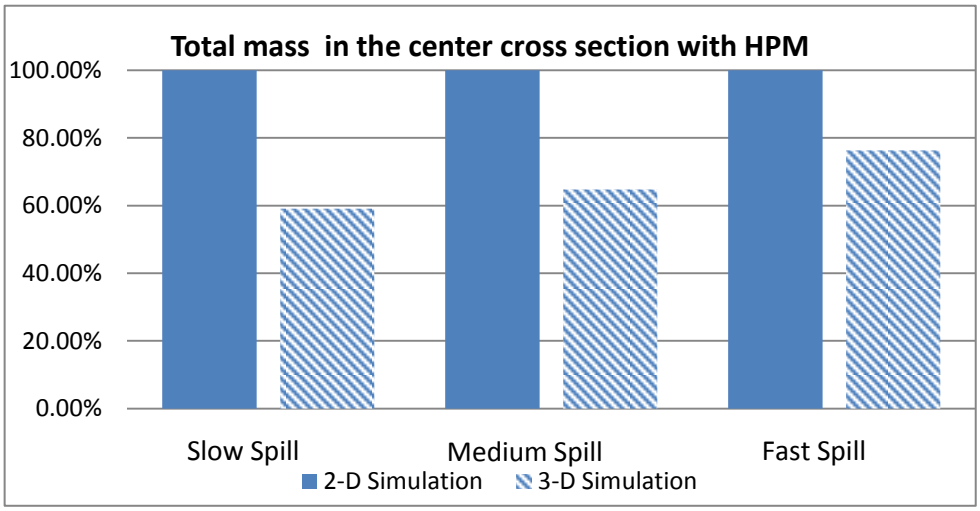

Figure 4.27 Percentage of mass in the center cross section with HPM

Figure 4.27 illustrates the percentage of mass left in the center cross section with HPM for 2-D and 3-D simulations. It can be noted that with HPM the percentage of mass left in the center cross sections is generally higher for 3-D simulations, comparing to that with Leverett scaling. Also, an increasing trend of mass left with increasing spill rates can be observed. For slow and medium spill rates the values for the percentage of mass are larger than 55% and 60%, and for fast spill rate the percentage of mass left in the center cross section for 3-D simulation is approaching 80%. The increasing trend of mass left in the center cross section with increasing spill rates seems contrary to what was observed in Figure 4.26, since Figure 4.26 reveals that at slower spill rate more PCE mass tend to pool at the lower region of the center cross section. However with the mean saturation value calculated for the three 3-D simulation results (0.051 for slow release, 0.055 for medium release, 0.067 for fast release), it is reasonable that more mass is left in the center cross section of the fast release even though less pooling occurs. Detailed discussions for each metric are as follows.

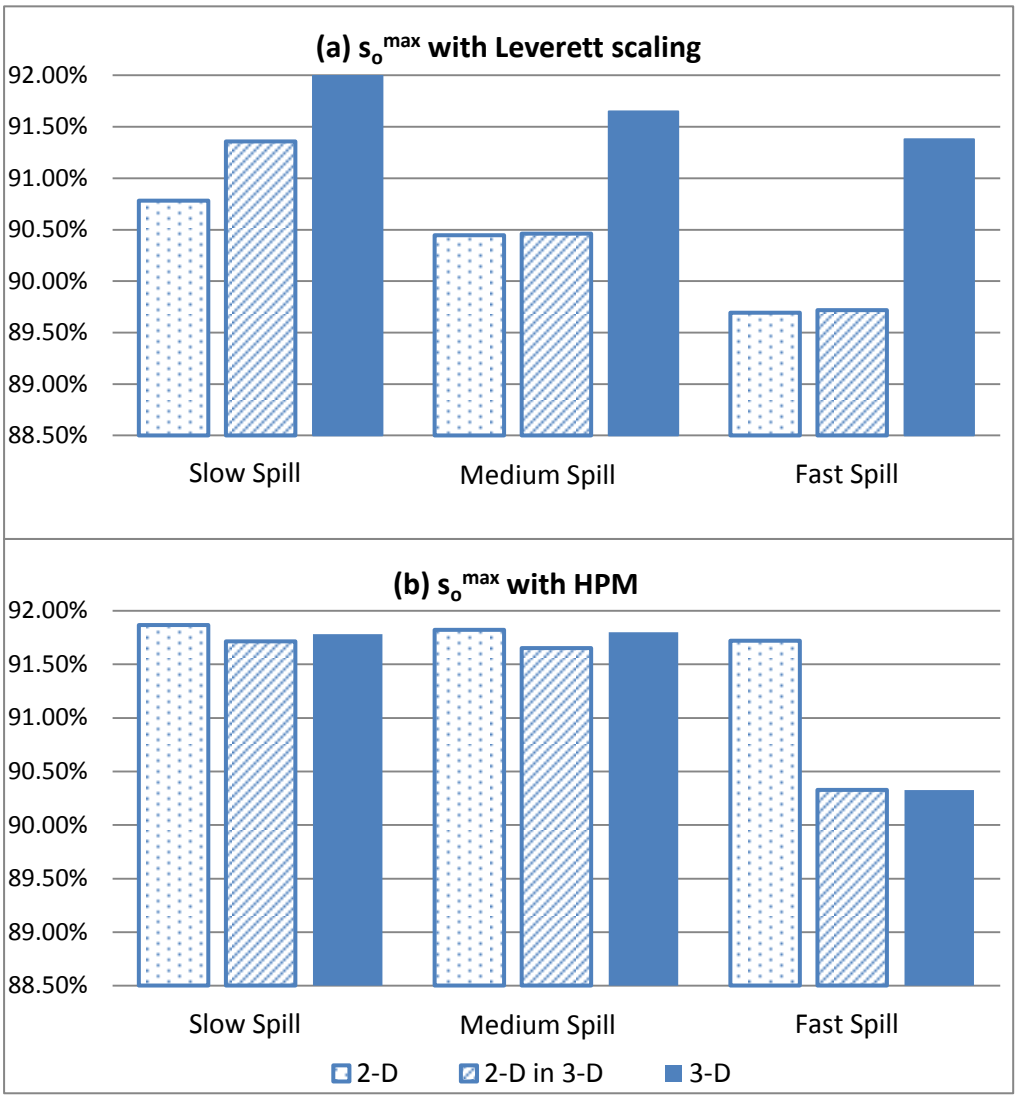

Figure 4.28 Comparison of s_o^{max} for 2-D and 3-D simulations with a) Leverett scaling and b) HPM

Christ et al. (2005) reported that s_o^{max} is insensitive to dimensionality for the mildly heterogeneous permeability field. Figure 4.28 reveals close estimates for s_o^{max} with either Leverett scaling or HPM for 2-D and 3-D simulations, with exception of the cases under slow release rate with Leverett scaling and fast release rate with HPM. In spite of the clear differences observed in Figure 4.28, it is observed that the 3-D and "2-D in 3-D" simulation results of s_o^{max} are only about 2.2% and 0.6% higher than 2-D simulation result with Leverett scaling under slow release respectively and, both about 1.5% smaller than 2-D

simulation result with HPM under fast release.

When analyzing s_o^{max}, the discrepancy between 2-D, "2-D in 3-D", and 3-D simulations is not obvious, and the influence of dimensionality on predicting s_o^{max} in highly heterogeneous permeability field is not significant.

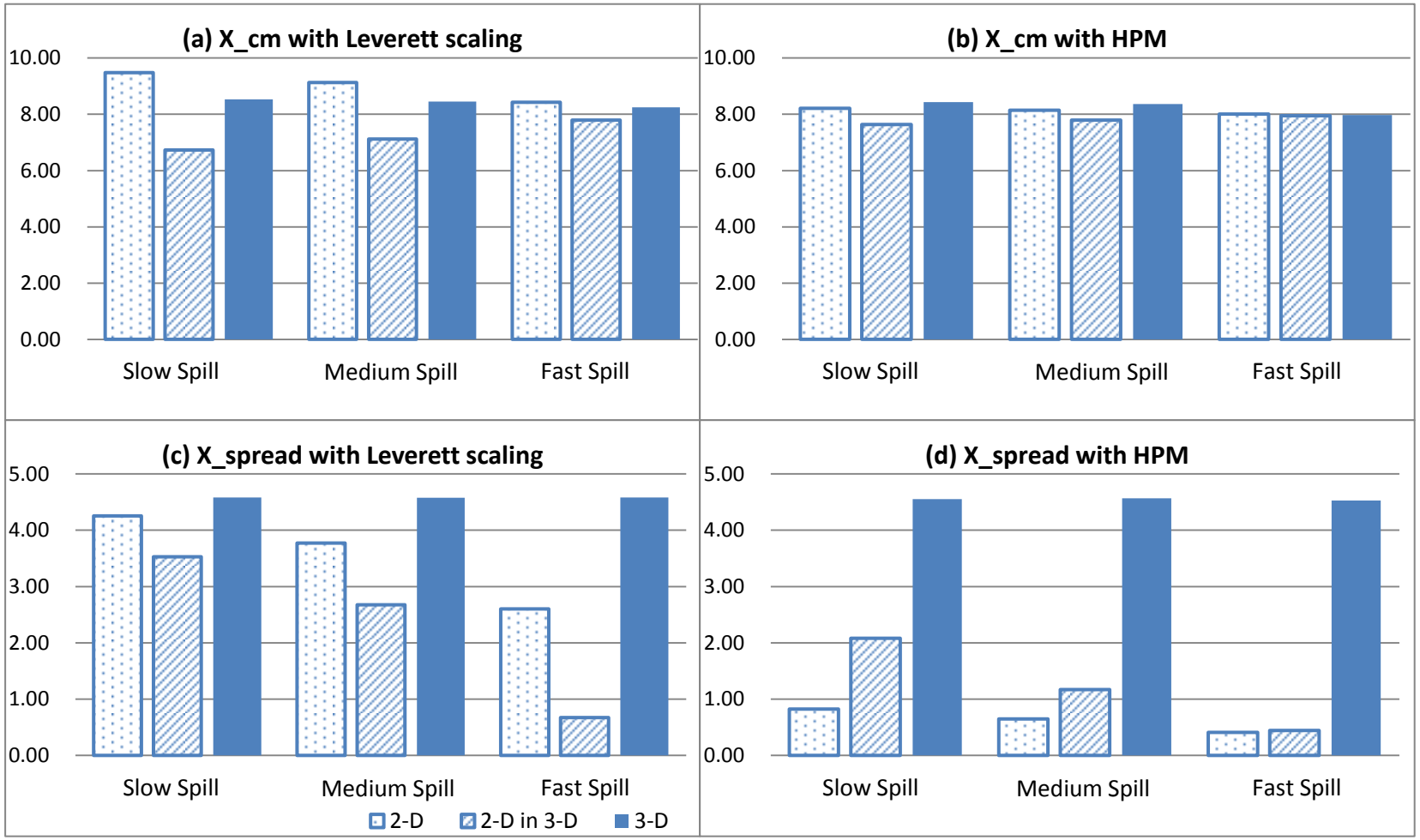

Figure 4.29 Comparison of x_{cm} and σ_{xx}^2 for 2-D and 3-D simulations with a), c) Leverett scaling and b), d) HPM

Figure 4.29 (a) reveals an inverse trend of x_{cm} with increasing spill rate among 2-D and "2-D in 3-D" simulation results when using Leverett scaling. 2-D simulation results for x_{cm} decreases with increasing spill rate, while "2-D in 3-D" simulation results for x_{cm} increases with increasing spill rate. This different trend indicates that the PCE pathways for 2-D and 3-D simulations in the center cross section are in different directions. But with increasing spill rate the PCE center of mass (x_{cm}) approaches to the center of the horizontal scale (8m) for both 2-D and "2-D in 3-D" simulations. The 3-D simulation results for x_{cm} is less sensitive to spill rate as 2-D and "2-D in 3-D" results. Figure 4.29 (b) shows that with HPM, the x_{cm} is not sensitive to spill rate for both 2-D, "2-D in 3-D", and 3-D simulation results, as there are no significant discrepancies between 2-D, "2-D in 3-D", and 3-D simulation results for x_{cm}. Since in 2-D and 3-D simulations the PCE pathways are different, the prediction of x_{cm} is influenced by the dimensionality, especially under slow release rate with Leverett scaling.

Figure 4.29 (c) and (d) reveal that with Leverett scaling, the 2-D simulations for σ_{xx}^2 are approximately 20% to 70% greater than "2-D in 3-D" simulation results, while with HPM the "2-D in 3-D" simulation results for σ_{xx}^2 are about 10% to 60% greater than 2-D simulations. Interestingly, with Leverett scaling, the difference of σ_{xx}^2 between 2-D and "2-D in 3-D" simulations tends to increase with increasing spill rate and, with HPM the difference of σ_{xx}^2 between 2-D and "2-D in 3-D" simulations shows a reverse trend. Notice that the σ_{xx}^2 calculated from the entire 3-D domain shows relatively stable results with increasing spill rate and different sets of capillary pressure-saturation parameters, which differs from either 2-D or "2-D in 3-D"

results. Therefore, from Figure 4.29 (c) and (d), the influence of capillary pressure-saturation parameters, spill rate, and dimensionality on the prediction of σ_{xx}^2 can be observed.

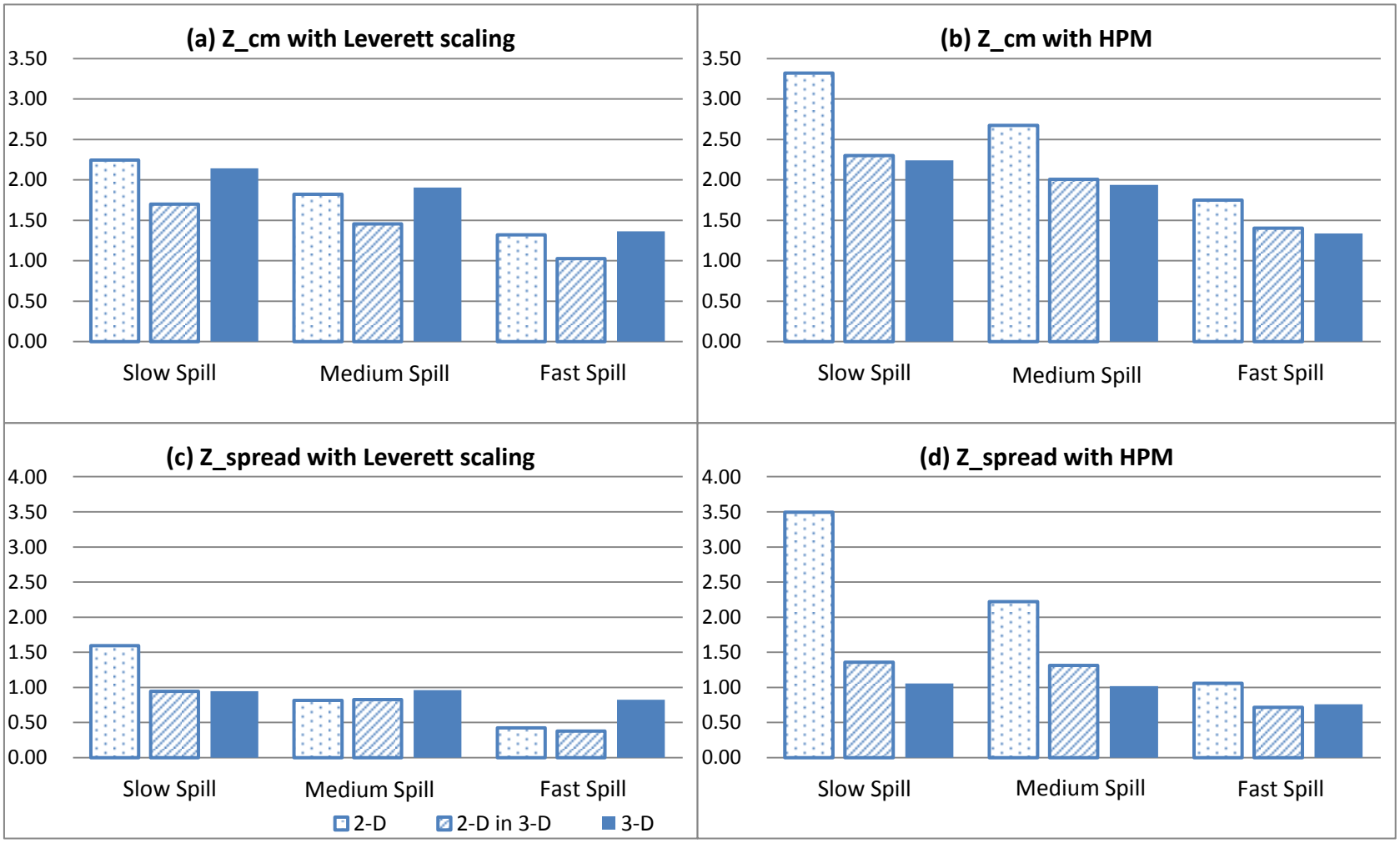

Figure 4.30 Comparison of z_{cm} and σ_{zz}^2 for 2-D and 3-D simulations with a), c) Leverett scaling and b), d) HPM

Comparing Figure 4.30 (a) and (b), it can be seen that with Leverett scaling, the simulation results for z_{cm} are smaller than those with HPM for 2-D, "2-D in 3-D", and 3-D simulation results. With leveret scaling, the 2-D simulation results for z_{cm} are approximately 20% to 25% higher than those for "2-D in 3-D" results and, very close to the 3-D results. With HPM, the 2-D simulation results for z_{cm} are about 20% to 30% higher than those for "2-D in 3-D" results, but the 3-D results are similar with "2-D in 3-D" results in this case. The 2-D, "2-D in 3-D", and 3-D simulation results for z_{cm} all exhibit a decreasing trend with increasing spill rates. Also, with increasing spill rates, the differences between 2-D and "2-D in 3-D" simulation results become smaller.

Figure 4.30 (c) and (d) show the same decreasing trend for σ_{zz}^2 with increasing spill rate for all the 2-D, "2-D in 3-D", and 3-D results using either Leverett scaling or HPM. With Leverett scaling, σ_{zz}^2 for 2-D simulation results are about 40% higher than "2-D in 3-D"results; but with increasing spill rate, the prediction of σ_{zz}^2 for 2-D and "2-D in 3-D" results become similar. When HPM is employed, σ_{zz}^2 estimated for 2-D simulation results are about 30% to 60% higher than "2-D in 3-D" results, even though the discrepancy becomes smaller with increasing spill rate. Again, the decreasing trend for σ_{zz}^2 calculated from the entire 3-D domain is not so obvious with increasing spill rate and capillary pressure-saturation parameters as 2-D and "2-D in 3-D" simulation results. From the above discussion, it can be concluded that with both Leverett scaling and HPM, dimensionality has a relatively strong influence on PCE vertical migration behavior.

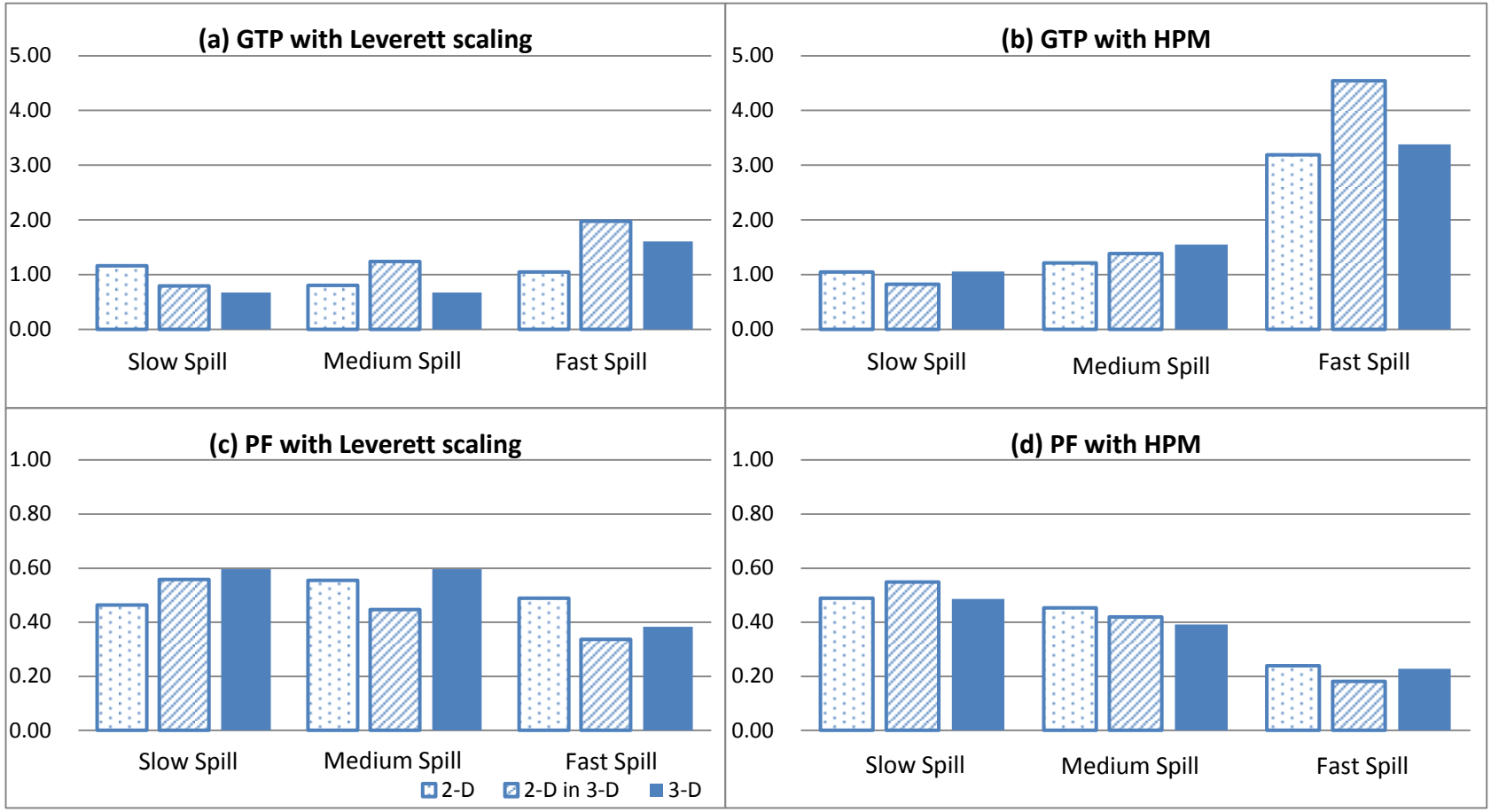

Figure 4.31 Comparison of GTP and PF for 2-D and 3-D simulations with a), c) Leverett scaling and b), d) HPM

Figure 4.31 (a) shows that for “2-D in 3-D” simulation results, the values of GTP increase with increasing spill rate when using Leverett scaling. However, for 2-D and 3-D simulation results with Leverett scaling, the GTP values obtained under medium spill rate are smaller than those with slow release. This could be an individual behavior for this realization, since we have observed an increasing trend of GTP with increasing spill rate in goal 2, even though the predictions of GTP for slow and medium release are close with Leverett scaling.

With HPM, there is a dramatic increase of GTP with increasing spill rate, and this trend is even more significant for “2-D in 3-D” simulation results than 2-D and 3-D results. As discussed in previous sections, the GTP and PF can be exchanged with each other, thus a reverse trend of spill rate can be observed on PF. Although the 3-D simulation results for GTP and PF show the same trend with spill rates as 2-D simulation results, the relationship of 2-D to 3-D simulations is unclear. It cannot be inferred whether the 2-D simulations for GTP and PF can be extended to 3-D simulation results for the highly heterogeneous permeability field from the study of a single realization. Before drawing a conclusion, a detailed study that includes the whole ensemble is necessary.

4.6 Goal 5: To compare simulated results for a highly heterogeneous aquifer with that for mildly heterogeneous aquifers

As explained in previous chapters, a number of numerical studies have explored the roles that soil properties and spill conditions play on the simulation of DNAPL infiltration and entrapment behavior in the subsurface (Dekker and Abriola, 2000; Lemke et al., 2004; Christ et al., 2005). These studies have been based on mildly heterogeneous permeability fields, such as the Bachman road site (Lemke et al. (2004)) and the Borden aquifer (Dekker and Abriola (2000)). The influence that capillary pressure-saturation parameters, residual organic saturation, and spill rate has on the simulation of DNAPL infiltration and entrapment in the highly heterogeneous aquifer for this study is assumed to be distinct from that for mildly heterogeneous aquifers.

Note that, the resolution of 0.25×0.1 m for the highly heterogeneous aquifer in this study is similar to the mildly heterogeneous aquifers for former studies (Dekker and Abriola (2000); Lemke et al. (2004)). Dekker and Abriola (2000) chose their grid spacing to be 0.5×0.1 m, and Lemke et al. (2004) limited their grid refinement to 0.3×0.08 m. Therefore, with the similar resolution of 0.25×0.1 m in this study, the dimensionless metrics, like the GTP, PF, and the maximum organic saturation, are comparable with the former studies. Detailed comparisons of different simulation conditions for highly heterogeneous versus mildly heterogeneous aquifers were conducted and explained below.

Similar to previous studies on mildly heterogeneous permeability fields, this

study demonstrated the important role that capillary pressure-saturation parameters play on the simulation of DNAPL infiltration and entrapment behavior in highly heterogeneous aquifer. Lemke et al. (2004) reported that the estimate of s_o^{max} tends to be larger and the range for s_o^{max} tends to be smaller when Leverett scaling is not adopted. In this study, although the results for s_o^{max} are generally very high when both Leverett scaling and HPM are used to determine the capillary pressure-saturation parameters, the same trend for the mean and range of s_o^{max} with that reported by Lemke et al. (2004) can be found. Results in chapter 4 show that with HPM, the values for s_o^{max} are higher and the ranges for s_o^{max} are smaller than those with Leverett scaling. Dekker and Abriola (2000) reported an increase of σ_{xx}^2 when the capillary pressure-saturation values are correlated with permeability using Leverett scaling, which is in agreement with the results for this study. For the highly heterogeneous aquifer studied here, the values for σ_{xx}^2 obtained with Leverett scaling are all greater than those obtained with HPM. Dekker and Abriola (2000) concluded that the correlation of capillary pressure-saturation parameters to the permeability field results in decreased z_{cm}. This conclusion can also be applied to the highly heterogeneous permeability field by noticing that the mean values for z_{cm} are greater with HPM than those with Leverett scaling. When using HPM, the capillary pressure-saturation parameters are assigned according to grain size distribution, therefore the capillary pressure-saturation parameters from HPM are not correlated with permeability.

On the other hand, Dekker and Abriola (2000) found that the correlation of residual organic saturation to permeability field had little influence on DNAPL

migration. In this study, in spite of the much higher heterogeneity and the large s_o^{max} obtained, the residual organic saturation had almost no influence on the prediction of the DNAPL source zone architecture.

The spill rate shows a distinct influence on the DNAPL migration in the highly heterogeneous permeability field compared to the mildly heterogeneous aquifer. Lemke et al. (2004) reported that increasing spill rate results in higher s_o^{max} and decreased spread. In this study, s_o^{max} tends to decrease with increasing spill rates. This trend for s_o^{max} in the highly heterogeneous aquifer could be attributed to the interplay between heterogeneity and spill rate, as Dekker and Abriola (2000) demonstrated that the increase of heterogeneity can obscure the influences that the spill rate plays on DNAPL migration. On the other hand, the spread, either horizontal or vertical, decreases with increasing spill rate, which is in agreement with what was observed in mildly heterogeneous aquifer reported by Lemke et al. (2004) and Dekker and Abriola (2000). Another agreement between mildly and highly heterogeneous aquifers can be found in z_{cm}. With increasing spill rate, the value of z_{cm} tends to be smaller for both mildly and highly heterogeneous aquifer. Dekker and Abriola (2000) and Lemke et al. (2004) did not show the influence of spill rate on GTP and PF, so there is no reported information to compare these metrics with those for mildly heterogeneous aquifers.

For mildly heterogeneous permeability fields, Christ et al. (2005) concluded that 2-D simulations tend to predict increased lateral and vertical spread and higher s_o^{max}, which is only partly consistent with what was observed with the simulations in highly heterogeneous permeability field. Christ et al. (2005)

scaled their entry pressure P_b with the permeability field, so only comparison of simulation results with Leverett scaling between this study and their results was conducted. For this highly heterogeneous aquifer, 2-D simulations gave higher σ_{zz}^2 and larger vertical penetration compared to those for 3-D simulations, which agree with the results in the mildly heterogeneous aquifer. However, contrary to their results, the s_o^{max} obtained from 2-D and 3-D simulations are similar (except slow release with Leveret scaling) and do not show a higher value for 2-D when compared to 3-D as observed in Christ et al. (2005). Since the s_o^{max} predicted for a highly heterogeneous aquifer is generally high (approaching the upper limit), the heterogeneity could be a reason that contributes to the close estimation for s_o^{max}. In addition, Christ et al. (2005) reported that in 2-D simulations, higher levels of mass are trapped in pools, which means that the GTP value for 2-D simulations should be smaller than 3-D simulations. In our study, there is a general trend that GTP values obtained from 2-D simulations are close to 3-D simulations, except those under slow release rate. To investigate the feasibility to extend 2-D results to 3-D simulations, a more detailed study with the whole ensemble is needed. Moreover, since the simulated metrics with Leverett scaling show a different trend than those with HPM in the highly heterogeneous aquifer, the conclusion for Christ et al. (2005) cannot be simply applied to the highly heterogeneous aquifer.

To compare the values of x_{cm}, z_{cm}, σ_{xx}^2, and σ_{zz}^2 for highly heterogeneous aquifer to those for mildly heterogeneous aquifers, these metrics were normalized according to the corresponding scale for the respective domain and converted into dimensionless quantities, as explained in Chapter 3. The

dimensionless quantities for each work are listed in Table 4.2.

Table 4.5 Dimensionless mean source zone metrics for highly and mildly heterogeneous aquifers

	s_o^{max}	x_{cm}	z_{cm}	σ_{xx}^2	σ_{zz}^2
This study (Herten site) (80L 0.5 L/day)	0.9018	0.562	0.370	0.019	0.049
This study (Herten site) (80L 20 L/day)	0.8885	0.519	0.214	0.008	0.016
Dekker and Abriola (2000) (Borden site) (75L 15 L/day)	0.0743	_	0.188	_	0.006
Christ et al. (2005) (Oscoda site) (32L 0.16 L/day)	0.354	0.472	0.331	0.014	0.026
Lemke et al. (2004) (Bachman Road site) (96L 0.24 L/day)	0.37	_	0.353	0.001	0.045

All the values present in Table 4.5 are adjusted from the mean values of the simulations with Leverett scaling (e.g. case 5 and 9 for this study, set 2 for Lemke et al. (2004)). Inspecting Table 4.5, it can be seen that the s_o^{max} obtained in highly heterogeneous aquifers are dramatically higher than those in mildly heterogeneous aquifers. In addition, the values for horizontal and vertical spread in highly heterogeneous aquifers are generally greater than those in mildly heterogeneous aquifers. The center of mass along horizontal direction is similar for mildly and highly heterogeneous aquifers since the release areas are located at the center of the simulated region for all the studies. z_{cm} for highly heterogeneous aquifer tends to be 10% to 30% higher than those for mildly heterogeneous aquifers. However, since there is neither the same volume nor same release rate for PCE in all the studies compared in Table 4.5, this result for z_{cm} may not be useful.

Chapter 5: Overall Conclusion and Future Direction

This study explored the infiltration and entrapment behavior of PCE in the subsurface of a highly heterogeneous glaciofluvial aquifer. The influence and impacts of the input parameters (capillary pressure-parameters, residual organic saturation, and spill rate), permeability field structure, and dimensionality on the numerical model predictions for DNAPL source zone configuration metrics were investigated. 2-D simulations were performed using a block centered, finite difference simulator M-VALOR for 10 sets of ensembles. Each ensemble contained 20 realizations and had different combinations of potentially significant input parameters. The metrics that describe the source zone architecture were calculated statistically for the 20 realizations and were compared between each set to investigate the influence of the input parameters and the field structure on the model prediction. These metrics include the maximum organic saturation, the horizontal and vertical center of mass, the horizontal and vertical spread of mass, ganglia to pool ratio, and the pool fraction. In addition, 3-D simulations for selected sets of input parameters were performed using UTCHEM to explore the influence of dimensionality on DNAPL migration.

The simulation results of each metric for this heterogeneous aquifer were compared with their counterparts for the mildly heterogeneous aquifers. The traditional variogram approach was used to reconstruct the mildly heterogeneous permeability field, in which the high textual contrast and laterally continuous stratigraphy were not present (Kueper and Frind, 1991b; Kueper and Frind, 1995; Dekker and Abriola, 2000; Lemke et al., 2004; Christ

et al., 2005, 2006, 2010). Accordingly, the extensive pooling of DNAPL that is commonly found in the field cannot be observed within the studies in mildly heterogeneous aquifers. This study employed the TP/MC method to reconstruct the permeability field and successfully preserved the laterally continuous stratigraphy and sufficient textural contrast. As a result, a larger extent of pooling can be observed for the simulations in the highly heterogeneous aquifer.

The simulations in this highly heterogeneous permeability field showed a strong influence of the method for determining of capillary pressure-saturation parameters on organic distribution. In agreement with the results for a mildly heterogeneous permeability field, higher order correlation of capillary pressure-saturation parameters to the permeability field can lead to an increase in σ_{xx}^2 and decrease in z_{cm} within the highly heterogeneous aquifer. The capillary pressure-saturation parameters affect the ratio of mass present in ganglia and pools. On the other hand, the correlation of the maximum residual organic saturation to permeability does not show the expected significant effects on DNAPL migration behavior in highly heterogeneous aquifers, even when extremely high s_o^{max} values were achieved.

Model predictions demonstrated a strong effect of the spill rate on the simulation of DNAPL migration. Trends observed in the highly heterogeneous aquifers, that the DNAPL mass tends to be trapped in the center areas and less spread occurs with increasing release rate agreed with trends observed for mildly heterogeneous aquifers. The overall average organic saturation tends to increase with increasing spill rate since the same amount of DNAPL mass was

released into the subsurface. What was different from previous studies with mildly heterogeneous aquifers (Dekker and Abriola, 2000; Lemke et al., 2004) is the prediction of s_o^{max}. While in mildly heterogeneous aquifers s_o^{max} tends to increase with larger spill rates, this study showed a reducing trend of this metric with increasing spill rates in highly heterogeneous aquifer. This discrepancy is attributed to the increase in heterogeneity, which is assumed to obscure the effects of spill rate on the DNAPL migration.

The permeability field structure exhibits a significant influence on simulations of PCE migration. Although the field structure does not strongly influence the prediction of s_o^{max}, the locations where the capillary barriers are present have a direct effect on the vertical penetration and horizontal spread of DNAPL mass. The permeability structure of the formation also affects the locations and extent of DNAPL pools. As a result, when generating the hypothetical field realizations, the TP/MC approach has to be carefully designed to capture known permeability observation.

The influence of dimensionality was briefly investigated due to the time limit for this study. Results showed that the dimensionality has different effects with Leverett scaling and HPM. With HPM, the predictions for s_o^{max}, x_{cm}, and PF are close for 2-D and 3-D simulations, while with Leverett scaling, the prediction for z_{cm} and σ_{zz}^2 are similar between 2-D and 3-D simulations. In general, the 3-D simulations express the same trend with increasing spill rates for every metric in comparison to 2-D simulations. However, it cannot be generalized that the 2-D simulation results for each metric are greater than 3-D simulation results as reported by Christ et al. (2005). In conclusion, based on

the aquifer realization in this study, the results for 2-D simulations should not be extended to 3-D simulations in highly heterogeneous aquifers.

Future work is needed for a more systematic study of 3-D behavior in highly heterogeneous permeability fields. Full ensemble sets of 3-D simulations and statistical analyses should be performed to investigate the extension of 2-D simulations to 3-D simulations within highly heterogeneous aquifers. Moreover, since the dissolution behavior and persistent period of DNAPL in the subsurface is governed by the source zone architecture, further investigations should include the dissolution behavior of the source zone obtained in this highly heterogeneous aquifer.

Chapter 6: References

Abriola, L.M. and Pinder, G.F., 1985. A multiphase approach to the modeling of porous media contamination by organic compounds, I. Equation development. Water Resour. Res., 21(1): l 1-18.

Abriola, Linda M., K. Rathfelder, M. Maiza, and S.Yadav. 1992. VALOR_Code_Version_1[1].0.pdf. Ann Arbor, Michigan.

Basu, Nandita B, P S C Rao, Irene C Poyer, M D Annable, and K Hatfield. 2006. "Flux-based assessment at a manufacturing site contaminated with trichloroethylene." Journal of contaminant hydrology 86 (1-2) (June 30): 105-27. doi:10.1016/j.jconhyd.2006.02.011. http://www.ncbi.nlm.nih.gov/pubmed/16581154.

Bayer, P., P. Huggenberger, P. Renard, and a. Comunian. 2011. "Three-dimensional high resolution fluvio-glacial aquifer analog: Part 1: Field study." Journal of Hydrology 405 (1-2) (July): 1-9. doi:10.1016/j.jhydrol.2011.03.038. http://linkinghub.elsevier.com/retrieve/pii/S0022169411002186.

Bradford, Scott a., Linda M. Abriola, and Klaus M. Rathfelder. 1998. "Flow and entrapment of dense nonaqueous phase liquids in physically and chemically heterogeneous aquifer formations." Advances in Water Resources 22 (2) (October): 117-132. doi:10.1016/S0309-1708(98)00005-0. http://linkinghub.elsevier.com/retrieve/pii/S0309170898000050.

Carle, Steven F. 1999. "Transition Probability Geostatistical Software."

Christ, John A, C Andrew Ramsburg, Kurt D Pennell, and Linda M Abriola. 2010. "Predicting DNAPL mass discharge from pool-dominated source zones." Journal of contaminant hydrology 114 (1-4) (May 20): 18-34. doi:10.1016/j.jconhyd.2010.02.005. http://www.ncbi.nlm.nih.gov/pubmed/20227132.

Christ, John A., C. Andrew Ramsburg, Kurt D. Pennell, and Linda M. Abriola. 2006. "Estimating mass discharge from dense nonaqueous phase liquid source zones using upscaled mass transfer coefficients: An evaluation using multiphase numerical simulations." Water Resources Research 42 (11) (November 28). doi:10.1029/2006WR004886. http://www.agu.org/pubs/crossref/2006/2006WR004886.shtml.

Cohen, Robert M., and James W. Mercer. 1993. "DNAPL SITE EVALUATION" (U.S. Environmental Protection Agency, Ada, Oklahoma 74820).

Delshad, M., G.a. Pope, and K. Sepehrnoori. 1996. “A Compositional Simulator for Modeling Surfactant Enhanced Aquifer Remediation, 1 Formulation.” Journal of Contaminant Hydrology 23 (4) (August): 303–327. doi:10.1016/0169-7722(95)00106-9. http://linkinghub.elsevier.com/retrieve/pii/0169772295001069

DiFilippo, E. L., and M. L. Brusseau. 2011. “Relationship between Mass Flux Reduction and Source-Zone Mass Removal: Analysis of Field Data” 98(1-2): 22-35. doi:10.1016/j.jconhyd.2008.02.004.RELATIONSHIP.

Essaid, H. I., and M. Hess, K. 1993. Monte Carlo Simulations of Multiphase Flow Incorporating Spatial Variability of Hydraulic Properties. U.S. Geological Survey, 345 Middlefield Road, Mail Stop 421, Menlo Park, California 94025.

Falta, Ronald W, Suresh P Rao, and Nandita Basu. 2005. “Assessing the impacts of partial mass depletion in DNAPL source zones I. Analytical modeling of source strength functions and plume response.” Journal of contaminant hydrology 78 (4) (August): 259-80. doi:10.1016/j.jconhyd.2005.05.010. http://www.ncbi.nlm.nih.gov/pubmed/16019108.

Fasano, G., Franceschini, A. (1987). "A multidimensional version of the Kolmogorov–Smirnov test". Monthly Notices of the Royal Astronomical Society (ISSN 0035-8711) 225: 155–170.

Fure, Adrian D, James W Jawitz, and Michael D Annable. 2006. “DNAPL source depletion: linking architecture and flux response.” Journal of contaminant hydrology 85 (3-4) (May 30): 118-40. doi:10.1016/j.jconhyd.2006.01.002. http://www.ncbi.nlm.nih.gov/pubmed/16527371.

Haverkamp, R., and J. Y. Parlange (1986), Predicting the water-retention curve from particle-size distribution: 1. Sandy soils without organic matter, Soil Sci., 142, 325–339.

Heinz, J, Sybille Kleineidam, Georg Teutsch, and Thomas Aigner. 2003. “Heterogeneity patterns of Quaternary glaciofluvial gravel bodies (SW-Germany): application to hydrogeology.” Sedimentary Geology 158 (1-2) (May 5): 1-23. doi:10.1016/S0037-0738(02)00239-7. http://linkinghub.elsevier.com/retrieve/pii/S0037073802002397.

Hoag, George E., and Michael C. Marley. 1986. “Gasoline Residual Saturation in Unsaturated Uniform Aquifer Materials.” Journal of Environmental Engineering 112 (3): 586. doi:10.1061/(ASCE)0733-9372(1986)112:3(586). http://link.aip.org/link/JOEEDU/v112/i3/p586/s1&Agg=doi.

Imhoff, P.T., A.S. Mann, M. Mercer, and M. Fitzpatrick. 2003. Scaling DNAPL migration from the laboratory to the fi eld. J. Contam. Hydrol., 64(1-2):73-92.

Kaluarachchi, J. J., and J. C. Parker. 1992. "Multiphase Flow with a Simplified Model for Oil Entrapment." Transport in Porous Media 7: 1-14.

Kostic, B, a Becht, and T Aigner. 2005. "3-D sedimentary architecture of a Quaternary gravel delta (SW-Germany): Implications for hydrostratigraphy." Sedimentary Geology 181 (3-4) (November 15): 147-171. doi:10.1016/j.sedgeo.2005.07.004. http://linkinghub.elsevier.com/retrieve/pii/S0037073805002423.

Kueper, Bernard H., and Emil O. Frind. 1991a. Two-Phase Flow in Heterogeneous Porous Media 1. Model Development. Water Resources Research.

Kueper, Bernard H., and Emil O. Frind. 1991b. Two-Phase Flow in Heterogeneous Porous Media 2. Model Application. Water Resources Research. Water Resources Research. doi:10.1029/91WR00267. http://www.agu.org/pubs/crossref/1991/91WR00267.shtml.

Kueper, Bernard H., David Redman, Robert C. Starr, Stanley Reitsma, and May Mah. 1993. A Field Experiment to Study the Behavior of Tetrachloroethylene Below the Water Table: Spatial Distribution of Residual and Pooled DNAPL. Ground Water.

Kueper, B.H. and J.L. Gerhard, 1995. Variability of point-source infiltration rates for two-phase flow in heterogeneous porous media. Water Resour. Res. 31(12), 2971-2980.

Land, C. S. (1968), Calculation of imbibition relative permeability for two- and three-phase flow from rock properties, Soc. Pet. Eng. J., 8, 149– 156.

Lee, Si-Yong, Steven F. Carle, and Graham E. Fogg. 2007. "Geologic heterogeneity and a comparison of two geostatistical models: Sequential Gaussian and transition probability-based geostatistical simulation." Advances in Water Resources 30 (9) (September): 1914-1932. doi:10.1016/j.advwatres.2007.03.005. http://linkinghub.elsevier.com/retrieve/pii/S0309170807000395.

Lemke, Lawrence D. 2004. "Dense nonaqueous phase liquid (DNAPL) source zone characterization: Influence of hydraulic property correlation on predictions of DNAPL infiltration and entrapment." Water Resources Research 40 (1): 1-16. doi:10.1029/2003WR001980. http://www.agu.org/pubs/crossref/2004/2003WR001980.shtml.

Lemke, Lawrence D., and Linda M. Abriola. 2006. "Modeling dense nonaqueous phase liquid mass removal in nonuniform formations:

Linking source-zone architecture and system response." Geosphere 2 (2): 74. doi:10.1130/GES00025.1. http://geosphere.gsapubs.org/cgi/doi/10.1130/GES00025.1.

Lenhard, R. J., J. C. Parker, and J. J. Kaluarachchi. 1989. A Model for Hysterestic Constitutive Relations Governing Multiphase Flow 3. Refinements and Numerical Simulations. Water Resources Research.

Leverett, M. C. (1941), Capillary behavior in porous solids, Pet. Dev. Technol., 142, 152– 169.

Liu K., 2001. Numerical modeling for DNAPL source characterization, PhD Thesis, Carnegie Mellon University, Pittsburgh, Pennsylvania.

Maji, R. 2005. "Conditional Stochastic Modeling of DNAPL Migration and Dissolution in a High-resolution Aquifer Analog." A thesis present to the University of Waterloo in fulfillment of the thesis requirement for the degree of Doctor of Philosophy in Earth Sciences.

Maji, R, E a Sudicky, S Panday, and G Teutsch. 2006. "Transition probability/Markov chain analyses of DNAPL source zones and plumes." Ground water 44 (6): 853-63. doi:10.1111/j.1745-6584.2005.00194.x. http://www.ncbi.nlm.nih.gov/pubmed/17087757.

Maji, R, and E a Sudicky. 2008. "Influence of mass transfer characteristics for DNAPL source depletion and contaminant flux in a highly characterized glaciofluvial aquifer." Journal of contaminant hydrology 102 (1-2) (November 14): 105-19. doi:10.1016/j.jconhyd.2008.08.005. http://www.ncbi.nlm.nih.gov/pubmed/18929427.

Mayer, A.S. and S.M. Hassanizadeh. 2005. Soil and Groundwater Contamination: Nonaqueous Phase Liquids. American Geophysical Union. Washington, D.C.

National Research Council. 2004. "Contaminants in the Subsurface: Source Zone Assessment and Remediation" (Committee on Source Removal of Contaminants in the Subsurface, National Academy of Science). http://www.nap.edu/catalog/11146.html.

Newell, Charles J., Richard L. Bowers, and Hanadi S. Rifai. 1994. "IMPACT OF NON-AQUEOUS PHASE LIQUIDS (NAPL S) ON GROUNDWATER REMEDIATION" (Summer National AICHE Meeting;, Symposium 23).

Pankow, J.F. and J.A. Cherry. 1996. Dense Chlorinated Solvents and Other DNAPLs in Groundwater. Portland: Waterloo Press

Pantazidou, Marina, and Ke Liu. 2008. "DNAPL distribution in the source zone: effect of soil structure and uncertainty reduction with increased sampling density." Journal of contaminant hydrology 96 (1-4) (February

19): 169-86. doi:10.1016/j.jconhyd.2007.11.002. http://www.ncbi.nlm.nih.gov/pubmed/18187230.

Park, E., and J.C. Parker. 2005. "Evaluation of an upscaled model for DNAPL dissolution kinetics in heterogeneous aquifers." Advances in Water Resources 28 (12) (December): 1280-1291. doi:10.1016/j.advwatres.2005.04.002. http://linkinghub.elsevier.com/retrieve/pii/S0309170805000916.

Parker, J. C., and E. Park. 2004. "Modeling field-scale dense nonaqueous phase liquid dissolution kinetics in heterogeneous aquifers." Water Resources Research 40 (5): 1-12. doi:10.1029/2003WR002807. http://www.agu.org/pubs/crossref/2004/2003WR002807.shtml.

Rathfelder, Klaus, and Linda M. Abriola. 1998. "The influence of capillarity in numerical modeling of organic liquid redistribution in two-phase systems." Advances in Water Resources 21 (2) (March): 159-170. doi:10.1016/S0309-1708(96)00039-5. http://linkinghub.elsevier.com/retrieve/pii/S0309170896000395.

Poulsen, M.M. and Kueper, B.H., 1992, A Field Experiment to Study the Behavior of Tetrachloroethylene in Unsaturated Porous Media, Environmental Science and Technology, v. 26 n. 5, pp. 889-895, ACS.

Powers, S.E., Abriola, L.M., Weber, W.J., 1992. An experimental investigation of nonaqueous phase liquid dissolution in saturated subsurface systems: steady state mass transfer rates. Water Resour. Res. 28 (10), 2691-2705.

Unger, A.J.A., (1995), Vacuum Extraction Coupled with Air Sparging for Remediation of Sandy Aquifers Contaminated by Volatile Chlorinated Solvents: A Multi-phase Compositional Approach. Thesis submitted to the University of Waterloo for the degree of PhD.

U.S.Environmetal Protection Agency. 1992. Estimating Potential for Occurrence of DNAPL at Superfund Sites. U.S. Environmental Protection Agency.

UTCHEM, 2000. Version 9.0 Technical Documentation. Center for Petroleum and Geosystems Engineering, The University of Texas at Austin, Austin, TX.

Wood, A Lynn, Carl G Enfield, Felipe P Espinoza, Michael Annable, Michael C Brooks, P S C Rao, David Sabatini, and Robert Knox. 2005. "Design of aquifer remediation systems : (2) Estimating site-specific performance and benefits of partial source removal B" 81: 148-166. doi:10.1016/j.conhyd.2005.08.004.